

#### **PAPER**

Insight into single-helix intelligent shape memory polymer cables: modeling and optimization under finite sliding contact

To cite this article: Alireza Enferadi et al 2024 Smart Mater. Struct. 33 055033

View the article online for updates and enhancements.

# You may also like

Distributions of stress and deformation in a braided wire rope subjected to tensile loading

Bao Song, Hui Wang, Weihua Cui et al.

 Intelligent visual detection method for the early surface damage of mine hoisting wire ropes

Ping Zhou, Gongbo Zhou, Hanyu Wang et

- Evaluation of latent variances in Monte Carlo dose calculations with Varian TrueBeam photon phase-spaces used as a particle source

Eyad Alhakeem and Sergei Zavgorodni



Smart Mater. Struct. 33 (2024) 055033 (21pp)

https://doi.org/10.1088/1361-665X/ad3bf9

# Insight into single-helix intelligent shape memory polymer cables: modeling and optimization under finite sliding contact

Alireza Enferadi<sup>1</sup>, Alireza Ostadrahimi<sup>2</sup>, Guoqiang Li<sup>2</sup>, Majid Baniassadi<sup>1</sup> and Mostafa Baghani<sup>1,\*</sup>

E-mail: lguoqi1@lsu.edu and baghani@ut.ac.ir

Received 1 September 2023, revised 5 January 2024 Accepted for publication 8 April 2024 Published 18 April 2024



#### **Abstract**

This pioneering study focuses on the finite element analysis (FEA) of thermomechanical properties of shape memory polymer (SMP) wire ropes and their components under both smalland finite-sliding contact deformation. To validate the FEA, we need to validate both geometric modeling and non-linear material behavior. Owing to intricate geometry, as well as excessive wire interactions in the structure, this part is studied by simulating a  $1 \times 37$  steel wire rope and then comparing it with existing experimental data. To evaluate the response of non-linear material behavior, we employ the available numerical results to model the thermomechanical property of an SMP rectangular bar under a uniaxial test and then verify both constrained and unconstrained recovery behavior. After rigorous validation, two configurations of  $1 \times 7$  and  $1 \times 27$  SMP cables are modeled based on the thermo-visco-hyperelastic constitutive framework for acrylate polymer systems. Upon exerting an axially tensile load on these  $1 \times 7$  and  $1 \times 27$  SMP wire ropes, the response of force and shape recovery, as well as the normal and shear stress distributions, are measured under constrained and unconstrained conditions. For a deeper physical understanding, the influences of different temperature rates (5 and 1 °C min<sup>-1</sup>), inter-wire sliding frictional coefficient (0.1-0.6), and multiple-shape programming on the stress-strain-temperature relations of these SMP cables are also investigated. Furthermore, based on optimizing two cable factors of diameter and helix angle, and using the design of experiments method, the specific energy of a 1 × 6 SMP cable is maximized. Under different thermomechanical loadings, this study tries to cast light on the remarkable features and possible potential applications of these newly developed SMP actuators which may foster unparalleled advancements in various industries.

Keywords: shape memory polymer, wire rope, thermo-visco-hyperelastic, finite strain, multiple shape memory effect, smart cable, FEM

#### 1. Introduction

The necessity of dragging, hauling, lifting, hoisting, and holding objects in various engineering applications are of great

importance. Wire ropes are the most crucial instruments in meeting these demands due to their flexibility in the transverse direction and high strength in the axial direction to carry thermo-mechanical loadings as well as abrasion and corrosion resistance. They can also exhibit a remarkable level of safety upon any wire or strand failure and are still able to ensure the continuity of industrial and engineering operations. Thus,

<sup>&</sup>lt;sup>1</sup> School of Mechanical Engineering, College of Engineering University of Tehran, Tehran, Iran

<sup>&</sup>lt;sup>2</sup> Department of Mechanical and Industrial Engineering, Louisiana State University, Baton Rouge, LA 70803, United States of America

<sup>\*</sup> Authors to whom any correspondence should be addressed.

based on the different configurations of strands and wires within a wire rope cross-section, various applications, including mechanical power transmission, cable-stayed bridge, towing, vessel anchoring, and support of oil platforms, may be expected [1].

Accordingly, extensive investigations have been carried out in this field to gain an appropriate understanding of the conventional wire ropes and their mechanical characteristics subjected to diverse mechanical loading with different constructions. Costello [2] studied the mechanical response of conventional cables and wire interactions when subjected to both torsional and axial loads. The effects of tensile forces on the interwire contact deformation and frictional coefficient of a 1 × 7 cable were examined by Utting and Jones [3]. Their findings exhibited a negligible significance of these phenomena on the overall behavior of the cable strands. Additionally, Stanova et al [4, 5] developed a mathematical model to describe wire rope configurations with both single-helix and double-helix structures, highlighting its notable effectiveness in facilitating the modeling of finite element analysis (FEA). In another study, Wang et al [6] employed the finite element method (FEM) to evaluate a  $19 \times 6$  steel cable while considering its elastoplastic materials characteristics.

Although conventional cables provided ample industrial applications, with the advent of smart materials, in particular, shape memory alloys (SMAs), more robust mechanical properties have also emerged, promoting more operational usage. In addition to high corrosion resistance, high energy absorption, and adequate tensile strength, manufacturing wire ropes from SMA may also lead to the recovery of large strains upon inducing shape memory effect (SME) as well as superelastic features. Reedlunn *et al* [7, 8] studied the superelastic behavior of two Ni–Ti cables with the constructions of  $7 \times 7$  and  $1 \times 27$ . Their results revealed that the  $1 \times 27$  cable may demonstrate a superior performance by achieving a more significant recoverable strain compared to a  $7 \times 7$  configuration, while the  $7 \times 7$  cable exhibited a higher force capability.

Furthermore, Biggs and Shaw [9] examined the dynamic actuation of both cables design under repeated thermal cycles, confirming that the  $7 \times 7$  construction effectively scaled up the adaptive properties of SMA wires. Moreover, the low or high cyclic fatigue characteristics of the SMA cable were investigated by Ozbulut et al [10] and Sherif and Ozbulut [11]. In addition, Carboni et al [12] devised a phenomenological framework to characterize the behavior of SMA cables, demonstrating a desirable agreement between experimental data and simulation results. Fang et al [13] assessed the dissipative energy of an SMA cable subjected to diverse loadings and under relatively low strain rates. Shi et al [14] examined the fatigue behavior of 7 × 7 Ni–Ti cables upon varying two factors of temperature and strain amplitude, revealing a significant influence of these parameters on the equivalent viscous damping. Furthermore, conducting some experiments on a cable-net model, Yang et al [15] investigated the modal damping properties of a SMA strand as a cross-ties. Vahidi et al [1]. Conducted FEA to investigate the superelastic and SME of single and double helix SMA wire under tensile loading. Accordingly, these remarkable features associated with SMA cables have led to an increased focus on their usage in seismic applications, particularly in braces/dampers [16–18] and isolation bearings [19–23]. While SMA wire ropes attracted significant attention as an appropriate tool choice for several engineering applications [24, 25], it is time to move even further beyond and introduce another state-of-the-art smart instruments: shape memory polymer (SMP) cables.

SMPs are a category of intelligent materials which can be altered into a desired temporary form when a force from an external source is applied [26]. After removing both a stimulus and the external force, a temporary shape can be preserved, and the original configuration can be reinstated upon reintroducing the stimulus [27]. This remarkable feature of SMP enables them to effortlessly modify their shape and characteristics, preparing them well-suited enough for applications that demand flexibility, substantial recoverable strains, and superior force capabilities [28]. Notably, various stimuli, including temperature [29], magnetic fields [30], electrical fields [31, 32], light [33, 34], pH levels [35], moisture or water [36], and radiation [37], can trigger this shape change. SMP materials offer several distinct advantages compared to their SMA and conventional steel counterparts. These lightweight SME polymers are primarily desirable for weight-sensitive applications, particularly in the space industry and robotics [38]. These structures also exhibit several economic saving stages such as biodegradability, biocompatibility, and low manufacturing costs [39], making them highly applicable for aerospace [40, 41], biomedical [42], textile [43], and microfluidics [44] utilizations.

In recent years, SMP single wire or fiber has been studied for its applications as suture in closing cracks in polymer matrix [45], as vibration dampers [46, 47], and as artificial muscles by twist insertion in precursor SMP fibers [48]. A simple structural mechanics model has been developed to describe the reversible actuation of this type of artificial muscles made of twisted and coiled two-way SMP fibers [49]. The extensive investigations conducted on traditional and SMA cables, and SMP single fibers have laid the groundwork for exploring the prospects of SMP cables. Nevertheless, to the best of our knowledge, no previous investigation has been presented yet to employ SMPs as a wire rope system. Thus, this study introduces SMP materials to this system using different single-helix wire ropes under several stages of thermomechanical loadings. To this end, through FEA, interwire geometry and contact status are initially validated with existing results of  $1 \times 37$  conventional cables [5]. We then adopt a thermo-visco-hyperelastic constitutive model developed by Arrieta et al [50] as it offers a compelling combination of simplicity and congruity with the experiment to model material behavior of SMPs for both shape and stress recovery under uniaxial test. It is worth noting that the material used in their study was an acrylate polymer network, which was a thermoset SMP and could be stretched to 50% [50]. After the modeling verification, the thermo-mechanical properties of several single helix SMP cables with  $1 \times 7$  and  $1 \times 27$  configurations are explored. To evaluate the mechanical efficiency of SMP wire rope, some comparisons are conducted against equivalent solid SMP wires. The shape recovery capabilities of these cables are subsequently examined under various strain magnitudes. Following these evaluations, the induced stress recovery of these cables and their constituent components is measured. Furthermore, the effects of frictional coefficient and temperature ramp rates on their recovery behavior are analyzed, and characterization of the multiple SME behavior is carried out. In an attempt to propose a comprehensive study on the thermomechanical behavior of SMP, a  $1 \times 6$  SMP cable is finally optimized by utilizing the design of experiment (DOE) method and based on the amount of energy that might be absorbed before the whole cable failure and breaking.

This paper is organized as follows: section 2 examines the characteristics of wire ropes and their constructions. A thermo-visco-hyperelastic constitutive model to simulate SMP material behavior is briefly described in section 3, and the dual and multiple SME are also discussed in this section. Section 4 provides material and geometric modeling as well as FEA of several  $1 \times 37$  steel,  $1 \times 7$  and  $1 \times 27$  SMP cables. Section 5 is dedicated to presenting detailed results and discussions on the different thermomechanical loadings. Moreover, the optimization of  $1 \times 6$  SMP cable is studied in section 6. Conclusions and summary are drawn in section 7.

# 2. Wire rope construction and modeling

A wire rope is composed of intertwined strands twisted around a central core (figure 1). These strands, in turn, undergo diverse geometric arrangements encircling a central core strand. Determining wire rope structural characteristics relies on three fundamental constituents: lay, texture, and pitch. The concept of lay refers to the specific directionality in which the wires and/or strands are intricately coiled around a central core. Texture pertains to the internal configuration and disposition of the wires within each individual strand. Pitch denotes the precise length requisite for completing a full revolution of the wire rope.

In addition, wire rope labeling entails multiplying the sum of strands by the number of constituent wires in each strand (figure 2(a)). The wire diameter (d) and outer diameter (D) of the cable are illustrated in figures 2(b) and (c). In this study, we employ two single helix SMP wire ropes with  $1\times 7$  and  $1\times 27$  arrangements, wherein a single strand comprises 7 and 27 constituent wires, respectively. Furthermore, the  $1\times 37$  configuration of the steel wire rope is utilized to validate the modeling approach.

The geometric modeling of helical SMP cable structures can be defined with parametric equations proposed by Stanova

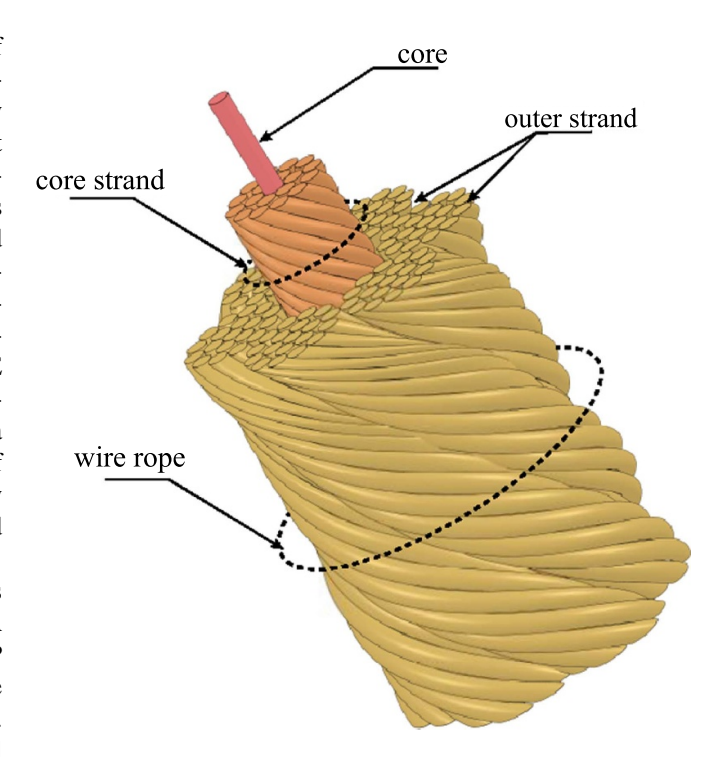


Figure 1. Various components of a wire rope.

et al [4], which specifically addresses the characteristics of helix wire ropes. The following parametric equations are employed to ascertain the coordinates of every point along a helical curve within the Cartesian coordinate system. By incorporating the helix angle represented as  $\varphi$ , the coordinates of points positioned on the helical curve can be accurately computed [4] as:

$$X(\varphi) = r_i \cos(q\varphi + \varsigma_{ii}) \tag{1}$$

$$Y(\varphi) = r_j \sin(q\varphi + \varsigma_{ij}) \tag{2}$$

$$Z(\varphi) = \varphi \frac{r_j}{\tan \alpha}.$$
 (3)

The parameter  $r_j$  signifies the radius of wires in the jth layer of a strand, whereas the variable  $\alpha$  represents the twist angle. Also, q indicates direction strands laid with +1 for right-hand lay and -1 for left-hand lay. The angle formed by center of the wire i in layer j with respect to the x-axis is indicated by the  $\varsigma_{ij}$  in equations (1)–(3) as:

$$\varsigma_{ji} = (i-1) \, \frac{2\pi}{n_i} \tag{4}$$

where  $n_j$  is the number of wires in layer j. Notably, the implementation of the derived geometric equations and the modeling of cables is facilitated through the utilization of the CATIA V5 software.

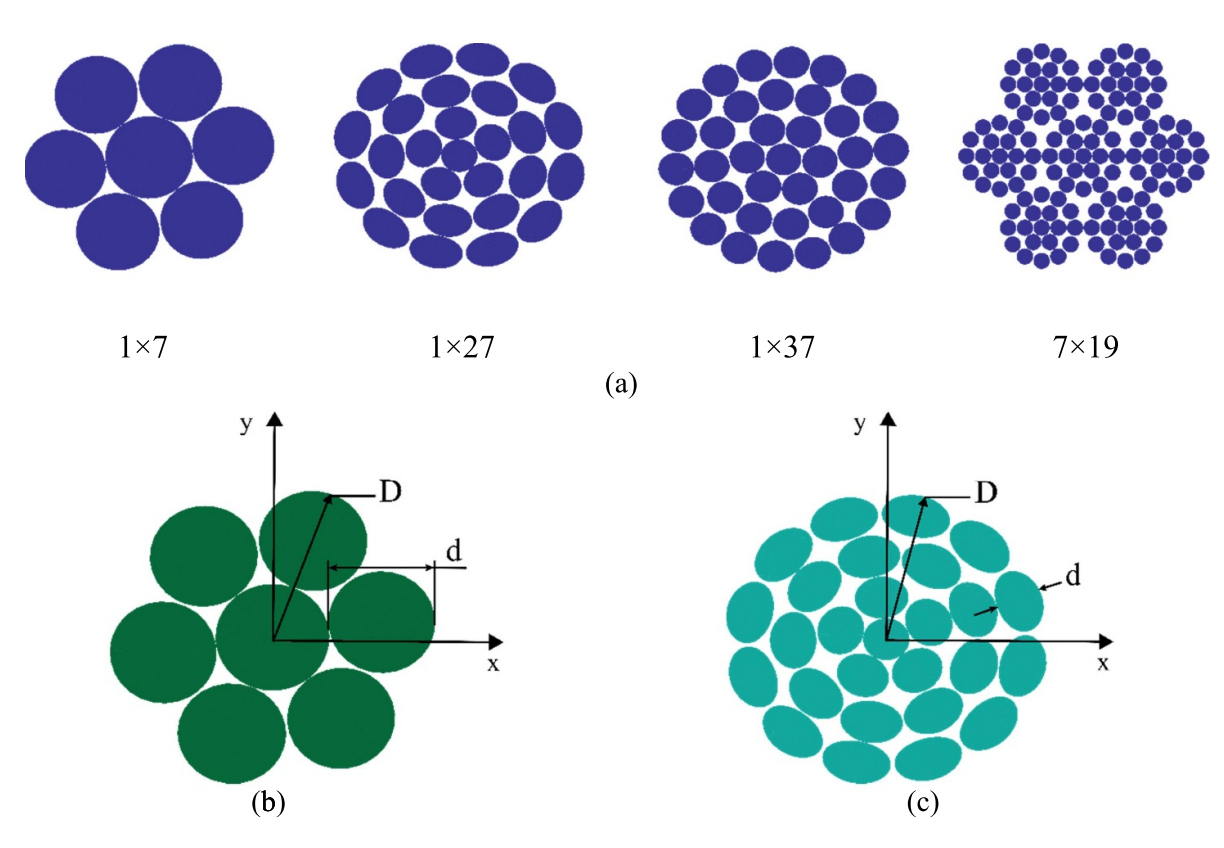


Figure 2. Characteristics of cables: (a) labeling, (b) cross-sectional geometry of  $1 \times 7$  configuration, and (c) cross-sectional geometry of  $1 \times 27$  configuration.

# 3. SMP material description

#### 3.1. Constitutive equations of SMPs

Proposed constitutive equations of SMP in the literature predominantly center on phase transitions and thermoviscoelastic methodologies [51]. The phase transition modeling approach considers SMPs to possess distinct phases, namely the glassy (frozen) and rubbery (active) states; however, the second approach is a physically-based view that considers inherent material properties, such as molecular interactions and relaxation, enabling better SMP behavior description and potential inclusion of phenomena like aging or solution-driven effects [52]. This approach was first presented by Westbrook et al [53] and subsequently modified by Diani et al [54] and Arrieta et al [50]. Due to its efficacy in modeling deformation response and recovery processes (figure 3), this paper employs a well-established thermo-visco-hyperelastic model to accommodate large deformations response of SMP wire

Based on this framework, the mechanical response of SMP material arises from both elastic and viscous characteristics. Within the domain of finite strains, the elastic component can be characterized by employing a hyperelastic model, while the viscous contribution is effectively represented using Prony's series. The total Cauchy stress may be formulated as:

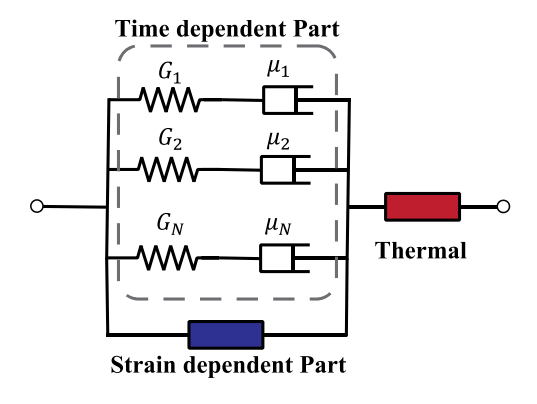


**Figure 3.** Schematic illustration of the rheological constitutive model proposed by Arrieta *et al* [50] for SMPs.

$$\boldsymbol{\sigma}\left(\boldsymbol{\varepsilon},t\right) = \int_{0}^{t} g\left(t-\xi\right) \frac{d\boldsymbol{\sigma}_{0}}{d\xi} d\xi \tag{5}$$

where  $\varepsilon$  and  $\sigma_0$  represent the total strain tensor and the stress associated with the instantaneous response of the material, respectively. Additionally, the nondimensional time-dependent part, denoted as g, is expressed in the form of Prony's series and storage modulus, G:

$$G(t) = G_{\infty} + \sum_{i=1}^{N} G_i e^{-\frac{t}{\tau_i}}$$
 (6)

$$G_0 = G_{\infty} + \sum_{i=1}^{N} G_i \tag{7}$$

in which  $G_0$ ,  $G_i$  and  $\tau_i$  are material parameters. The formulation of the storage modulus can be restated as:

$$G(t) = G_0 + \sum_{i=1}^{N} G_i \left( 1 - e^{-\frac{t}{\tau_i}} \right).$$
 (8)

In conclusion, g(t) can be described as:

$$g(t) = \frac{G(t)}{G_0} = 1 - \sum_{i=1}^{N} g_i \left( 1 - e^{-\frac{t}{\tau}} \right). \tag{9}$$

In essence,  $\sigma_0$  assumes the role of the hyperelastic component. Consequently, by utilizing the principles of hyperelasticity, it may be expressed as follows:

$$\boldsymbol{\sigma}_{0} = -p\mathbf{I} + 2\left(\frac{\partial\psi}{\partial I_{1}} + I_{1}\frac{\partial\psi}{\partial I_{2}}\right)\mathbf{B}_{M} - 2\frac{\partial\psi}{\partial I_{2}}\mathbf{B}_{M}^{2}$$
(10)

where p corresponds to the Lagrangian multiplier,  $\psi$  signifies the strain energy function and **B** denotes the left Cauchy–Green deformation tensor. Furthermore, M index serves as a denotation for the mechanical aspect of **B** as:

$$\mathbf{B}_M = \mathbf{F}_M \mathbf{F}_M^T \tag{11}$$

where the deformation gradient is denoted by **F**. Regarding the effect of thermal expansion, the following relationship can be established:

$$\mathbf{F}_T = \Lambda_T \mathbf{I} = (1 + \alpha_T (T - T_0)) \mathbf{I}$$
 (12)

in which the thermal expansion coefficient, denoted as  $\alpha_T$ , is a temperature-dependent parameter influenced by both temperature and the rate of temperature change. By employing the multiplicative decomposition for **F**, one can achieve:

$$\mathbf{F}_M = \mathbf{F} \mathbf{F}_T^{-1}. \tag{13}$$

Furthermore, by utilizing the Neo-Hookean strain energy function, the hyperelastic characteristics of the SMP can be effectively described as:

$$\psi = C_0 (I_1 - 3) \tag{14}$$

where  $C_0$  is a material parameter.

In order to incorporate the impact of temperature on the behavior of SMPs, particularly the phenomena of softening or stiffening, the utilization of the principle of time-temperature superposition (TTSP) is employed. Within this theoretical framework, a postulation is made regarding the correlation between temperature and the temporal aspect. Consequently, the William–Landel–Ferry (WLF) correlation accounts for

this phenomenon [55]. This study employs the WLF equation to modify the temporal scale appropriately

$$\log_{10} A_T = -\frac{c_1 (T - T_{\text{ref}})}{c_2 + (T - T_{\text{ref}})}$$
 (15)

where  $c_1$ ,  $c_2$  and  $T_{ref}$  are associated with material properties, and the reduced time,  $t_r$ , expressed as:

$$t_r(t) = \int_0^t \frac{d\eta}{A_{T(\eta)}}.$$
 (16)

Consequently, the total stress is redefined as:

$$\sigma\left(\varepsilon,t,T\right) = \int_{0}^{t} g\left(t_{r} - \xi_{r}\right) \frac{d\sigma_{0}}{d\xi} d\xi. \tag{17}$$

#### 3.2. Dual- and multi-SME

As illustrated in figure 4, SME can be described in a strain–stress–temperature diagram. The programming procedure begins at an elevated temperature  $T_H$  ( $>T_g$ ), characterized by unconstrained stress and strain conditions. Subsequently, the SMP is subjected to external loading while still exposed to a high temperature. Following this stage, the temperature should be reduced to  $T_C$  ( $<T_g$ ), while a strain is maintained to fix the new temporary shape. After stabilizing the temperature, the SMP material is unloaded to achieve the shape set after a small amount of spring back. However, the permanent shape can be restored by elevating the temperature to its initial level, denoted as  $T_H$ . This trajectory is commonly referred to as stress-free strain recovery. Conversely, maintaining a constant strain while increasing temperature in the recovery step leads to generating a force referred to as fixed-strain stress recovery.

Moreover, the multiple SME is a distinct type of shape memory phenomenon (figure 5) [50]. First, the SMP is heated from  $T_C$  to  $T_{H_1}$  (II). This heating process prepares the material for deformation. Next, the SMP undergoes deformation, allowing it to acquire a temporary shape (III). Once the desired temporary shape is achieved, the temperature is reduced while keeping the strain fixed, resulting in a new temperature  $T_{H_2}$ , which is lower than  $T_{H_1}$  (IV) [56, 57]. Despite the temperature reduction, the strain is maintained in the material. Following this, another deformation is applied to the SMP, leading to the formation of a new temporary shape (V) [56, 57]. The SMP is gradually cooled down to  $T_C$  while keeping the constraints intact, ensuring that the desired shape is maintained throughout the cooling process. Then the imposed constraints are removed throughout the unloading stage so that the SMP material effectively preserves both applied deformations within its memory (VII). Upon thermal exposure at  $T_C$ , the sample undergoes a transition into the temporary shape (V), known as the initial recovery (VIII) process. Subsequent temperature increments promote retrieving the original shape through a second recovery process (IX) [58].

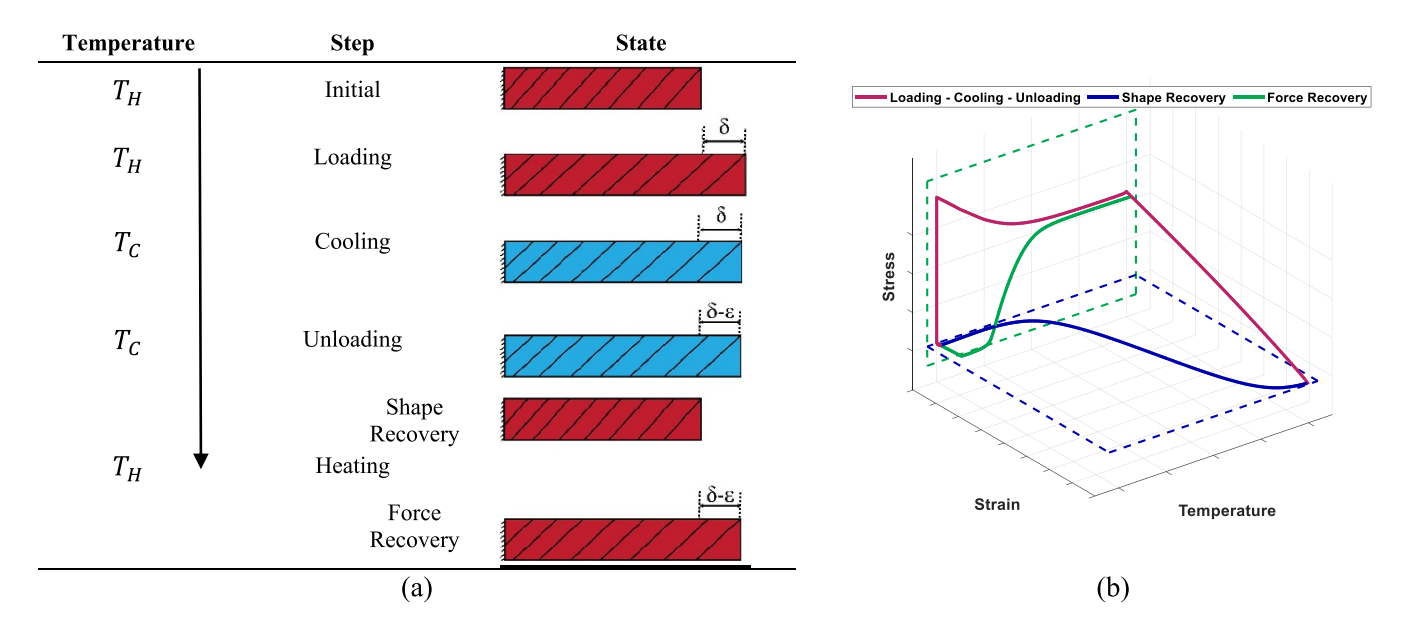


**Figure 4.** (a) Deformation schematic of an SMP wire rope in permanent and temporary shapes, (b) stress–strain–temperature diagram depicting the thermomechanical behavior of SMP.

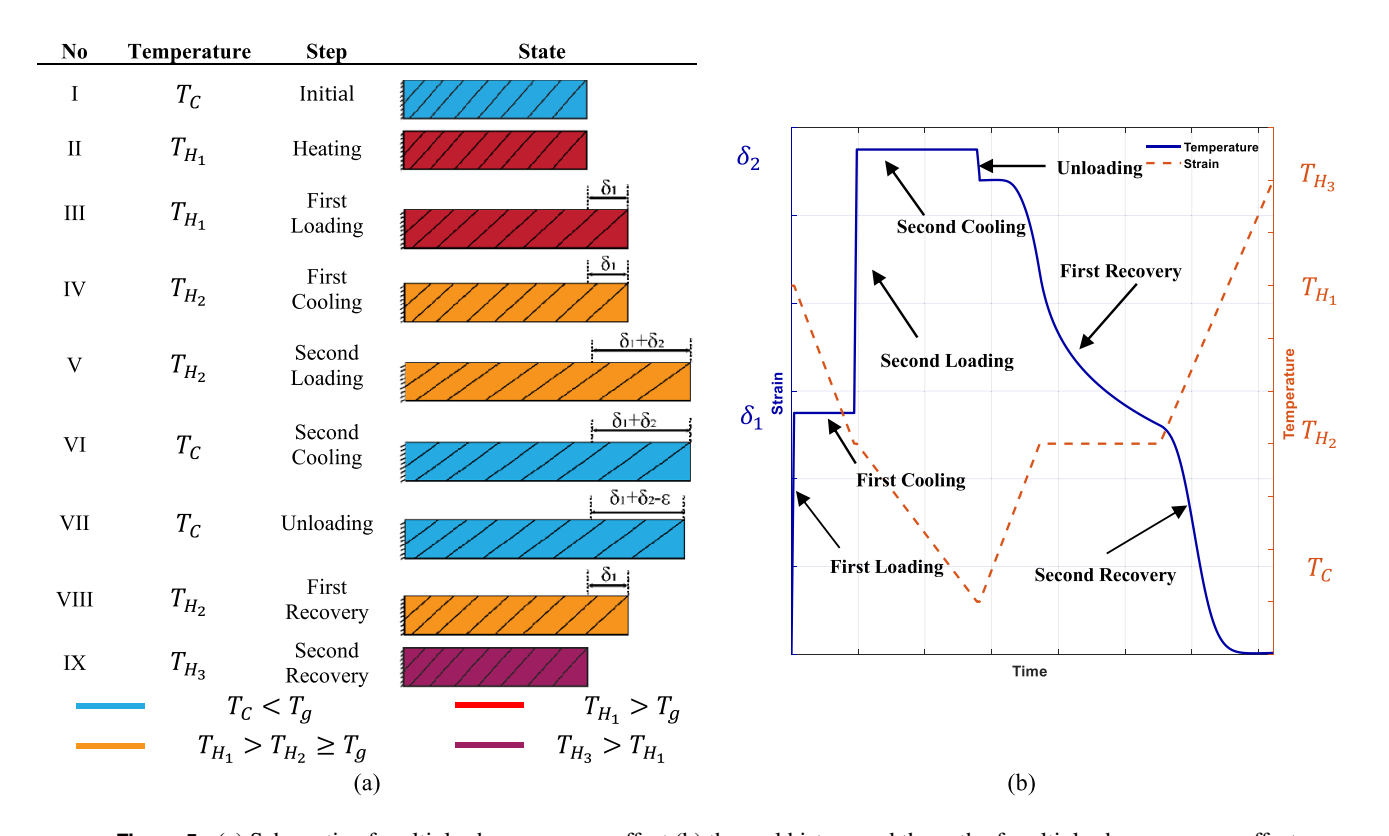


Figure 5. (a) Schematic of multiple shape memory effect (b) thermal history and the path of multiple shape memory effect.

# 4. Geometric and material verification of wire ropes with various constructions

This section aims to verify the modeling process and assess the wire-to-wire contact of cables with different cross-sectional configurations. The investigation employs the FEM for analyzing the behavior and performance of several single-helix SMP wire ropes with  $1 \times 7$  and  $1 \times 27$  arrangements. To

evaluate the accuracy of our analyses, we compare the results obtained from a  $1 \times 37$  steel model with the existing numerical model [5]. Additionally, the validity of the material model is confirmed by comparing it to experimental data [50]. For the FEA, the implicit solution is relatively more complex and time-consuming when compared to the explicit solution; nevertheless, this method yields higher precision in dynamic mode, thereby ensuring the accuracy of the results.

**Table 1.** Geometric attributes and material specifications of  $1 \times 37$  steel cable and its components. Reprinted from [5], Copyright (2011), with permission from Elsevier.

Instances $d \text{ (mm)}$		$\varphi (\deg)$	L(mm)
Core wire	1.09	_	67.00
First layer	1.00	10.77	68.19
Second layer	1.00	10.77	68.19
Third layer	1.00	10.77	68.19
	Material param	eters	
Parameters	Unit	Value	
Young modulus	GPa	190	
Passion ratio —		0.3	
Density kg m <sup>-</sup>		7850	

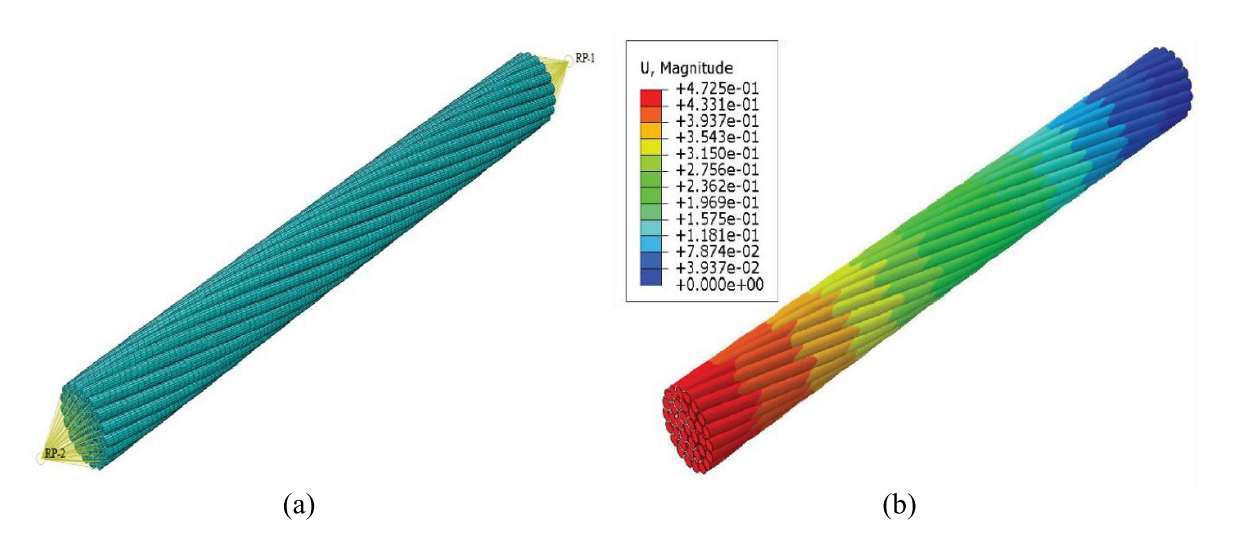


**Figure 6.** (a) FEM model of  $1 \times 37$  (b) displacement result for 35 kN force.

#### 4.1. Steel cable with a 1 $\times$ 37 configuration

In this model, the frictional coefficient interaction between neighboring wires is 0.2, and the geometric as well as material specifications of the steel cable are provided in table 1.

Employing a surface-to-surface contact approach, the interactions among the wires are considered in both the tangential and normal orientations with respect to the wire surface. Two reference points, denoted as RP-1 and RP-2 (figure 6(a)), are established along the central axis of the cable. These points are equidistant from the cable endpoints and induce a coupling effect among the nodal points for each cross-section. This kinematic coupling ensures that the strands within the cable exhibit identical displacements between these reference locations. Consequently, it restricts any relative motion between the wire cross-sections while permitting relative deformations between the interconnected surfaces. If the wire rope is of sufficient length to eliminate clamping effects, the degrees of freedom at reference point 2 can be fully constrained. On the other hand, at reference point 1, longitudinal movement can only occur by applying a tensile force that linearly varies with time.

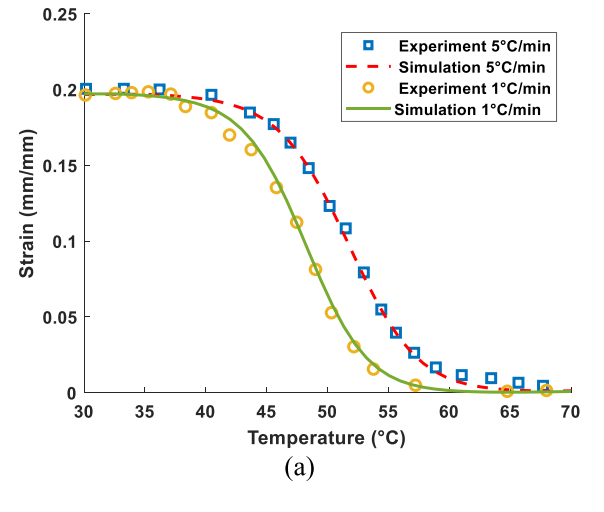
Utilizing C3D8R components of dimensions  $0.6 \times 0.2$  mm, the cable is discretized in the present investigation. A list of material properties employed in the simulation can be found in table 1. Figure 6(b) shows the distinct elongation values of individual components after applying a 35 kN force on a  $1 \times 37$  steel rope. The FEA incorporates various force magnitudes (10, 20, 30, and 35 kN). The obtained results are compared with the findings reported by Stanova *et al* [5], and this satisfactory assessment is presented in table 2.

#### 4.2. Validation of SMP material model

The material characteristics that Arrieta *et al* [50] earlier calibrated for large deformation and later validated through experimental observations have been utilized in the current study for a rectangular specimen ( $10 \times 1.6 \times 90$  mm). These material properties are implemented in the ABAQUS software to simulate the behavior of SMPs under uniaxial tension. Subsequently, the predictions are compared against experimental data to verify their agreement. Numerous thermomechanical cycles may exist for characterizing the shape memory behavior of such materials, so that dual shape memory cycle

Force (kN) Numerical result [5] (mm) Present work (mm) Error (%) 10 0.1505 0.1481 1.59 20 0.2749 0.2746 0.11 30 0.4080 0.4052 0.69 35 0.4728 0.4725 0.06

**Table 2.** Comparison of the cable elongation. Reprinted from [5], Copyright (2011), with permission from Elsevier.



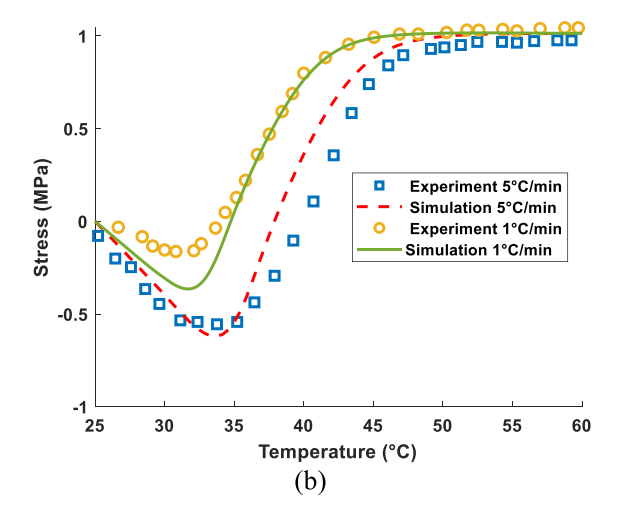


**Figure 7.** Comparison of SMP material model with experimental data for different temperature rates: (a) shape recovery of SMP under 20% applied strain in different temperatures, (b) stress recovery of SMP under 20% applied strain in different temperatures.

is the most widely used, comprising two unique modes: shape recovery and force (stress) recovery. Arrieta *et al* [50] studied an SMP under two temperature ramp rates (1 and 5  $^{\circ}$ C min<sup>-1</sup>), with optimum performance at 25 and 65  $^{\circ}$ C (low and high temperatures). The coefficients reported in table 3 are taken from their work.

The strain and stress recovery cycle during reheating is illustrated in figure 7. The model precisely predicted both free stress and fixed strain recovery across different loading states, thus, it might be a good candidate to simulate the response of wire rope SMP components under more complex loading conditions and geometries.

#### 4.3. SMP wire ropes (1 $\times$ 7 and 1 $\times$ 27)

To accurately simulate the mechanical properties of SMP cables, it is imperative to ensure that the cable lay length is sufficiently long to let each strand at least have one full turn around the core. Therefore, considering the maximum pitch of individual wires, the lengths of the  $1 \times 7$  and  $1 \times 27$  cables are determined to be 10 and 4 mm, respectively. The model is considered as a cantilever system, whereby deformation and axial tensile force are imposed using reference points 1 and 2 to follow the experimental setups. The presence of geometric nonlinearity during the loading and unloading stages necessitates incorporating wire interactions and contact modeling in both normal and tangential directions. Concerning figure 2(a), it is possible to calculate the number of interactions for a single helix cable [1] as:

$$N_s = \sum_{i=1}^{k} n_i + n_1 + \sum_{i=1}^{k-1} (n_i \times n_{i+1})$$
 (18)

where  $n_i$  denotes the number of wires in the ith layer, while k symbolizes the total number of complete layers. The material parameters, namely hyperelasticity, viscoelasticity, thermal expansion, and TTSP properties have been borrowed from Arrieta et al [50] in table 3. Furthermore, the frictional interactions between wire surfaces are characterized by a coefficient of 0.115. The  $1 \times 7$  and  $1 \times 27$  structures are meshed using 60 000 and 138 000 elements and feature dimensions of  $0.05 \times 0.05$  and  $0.03 \times 0.08$ , respectively (figure 8).

### 5. Results and discussion

The mechanical behavior of wire ropes hinges significantly on the interplay of wire interaction, which directly influences force distribution, displacement variation, and energy dissipation of these structures. A comparative assessment of the mechanical properties of SMP cables and solid SMP bars is presented in this section to discern the potential advantages of utilizing SMP cables over conventional solid bars. Regarding equivalent volume, the response of force and shape recovery for current SMP wire ropes may be independently compared with solid SMP bars. The thermomechanical performance of both SMP cables and solid SMP bars are thoroughly evaluated by a temperature rate of 5 °C min  $^{-1}$  under 20% strain. The resultant recovery profiles under both constrained

Table 3. Material parameters borrowed from Arrieta et al [50]. Reprinted from [50], Copyright (2014), with permission from Elsevier.

		,			,,,				
				Viscoelastic pro	Viscoelastic properties of SMP				
$\frac{g_1}{1.8706 \times 10^{-01}}$	$\frac{g_2}{1.5840\times 10^{-01}}$	$\frac{g_3}{1.3761 \times 10^{-01}}$	$\frac{g_4}{1.2378 \times 10^{-01}}$	$85 \\ 1.1283 \times 10^{-01}$	$^{g_6}_{9.8684\times10^{-02}}$	$^{87}_{7.5819 \times 10^{-02}}$	$\frac{g_8}{4.7521 \times 10^{-02}}$	$\frac{89}{2.4477 \times 10^{-02}}$	$\frac{g_{10}}{1.1615\times10^{-02}}$
$\frac{g_{11}}{5.8277\times10^{-03}}$	$\frac{g_{12}}{3.1994 \times 10^{-03}}$	$\frac{g_{13}}{1.8449 \times 10^{-03}}$	$\frac{g_{14}}{1.0527\times10^{-03}}$	$\frac{g_{15}}{5.6387\times10^{-04}}$	$\frac{g_{16}}{2.8586 \times 10^{-04}}$	$\frac{g_{17}}{1.4378 \times 10^{-04}}$	$g_{18}$ 7.4217 × $10^{-05}$	$\frac{g_{19}}{3.911 \times 10^{-0}.5}$	$\frac{g_{20}}{2.0746\times10^{-05}}$
$^{7_1}$ $1.26  imes 10^{-06}$	$^{72}$ 2.94 × $10^{-06}$	$ au_3$ 6.87 $ imes 10^{-06}$	$^{74}$ $1.60 \times 10^{-05}$	$^{75}$ 3.75 $ imes$ 10 $^{-05}$	$^{76}$ 8.78 × $^{10^{-05}}$	$^{77}$ 2.04 × $10^{-04}$	$^{78}$ 4.78 × $^{10^{-04}}$	$^{79}$ 1.12 × $10^{-03}$	$^{710}_{2.61\times10^{-03}}$
$7_{11} \\ 6.08 \times 10^{-03}$	$^{712}_{1.42\times10^{-02}}$	$^{\tau_{13}}_{3.32\times10^{-02}}$	$ au_{14}$ 7.75 × $10^{-02}$	$^{715}_{1.81\times10^{-01}}$	$^{716}$ 4.32 × $10^{-01}$	$^{\tau_{17}}_{9.88\times10^{-01}}$	$^{\tau_{18}}_{2.31\times10^{+00}}$	$ au_{19}  ext{5.39}  imes 10^{+00}$	$^{720}_{1.26\times10^{+01}}$
				Hyperelastic materi	Hyperelastic material parameter for SMP	ſ₽			
Strain energy potential Neo Hookean	ential						$C_0 (Pa)$ 109 730 000		
				WLF TTSP	WLF TTSP parameters				
	$T_{ m ref}\left(^{ m o}{ m C} ight)$			$C_1$ (	$C_{1}(-)$ 6.9			$C_2(^{ m o}{ m C}) \ 87.9$	
			The	Thermal properties of SMP at $\dot{T}=1^{\circ}C/\min$	SMP at $\dot{T} = 1^{\circ} C/n$	uin			
$\frac{T(^{\circ}\mathrm{C})}{\alpha_{T}\times10^{-4}}$	20	25 30 0.95 0.99	35	40	45 50 1.21 1.30	55 0 1.39	60 1.46	65 70 1.52 1.5	70 75 1.56 1.59
			Th	Thermal properties of SMP at $\dot{T}=5^{\circ}\text{C}/\text{min}$	SMP at $\dot{T} = 5^{\circ} \text{C/ n}$	uin			
$T(^{\circ}\mathrm{C})$			35	40			09		
$\alpha_T \times 10^{-4}$	1.17	1.22 1.26		1.41	1.5	) 1.67	1.73	1.78 1.8	1.82

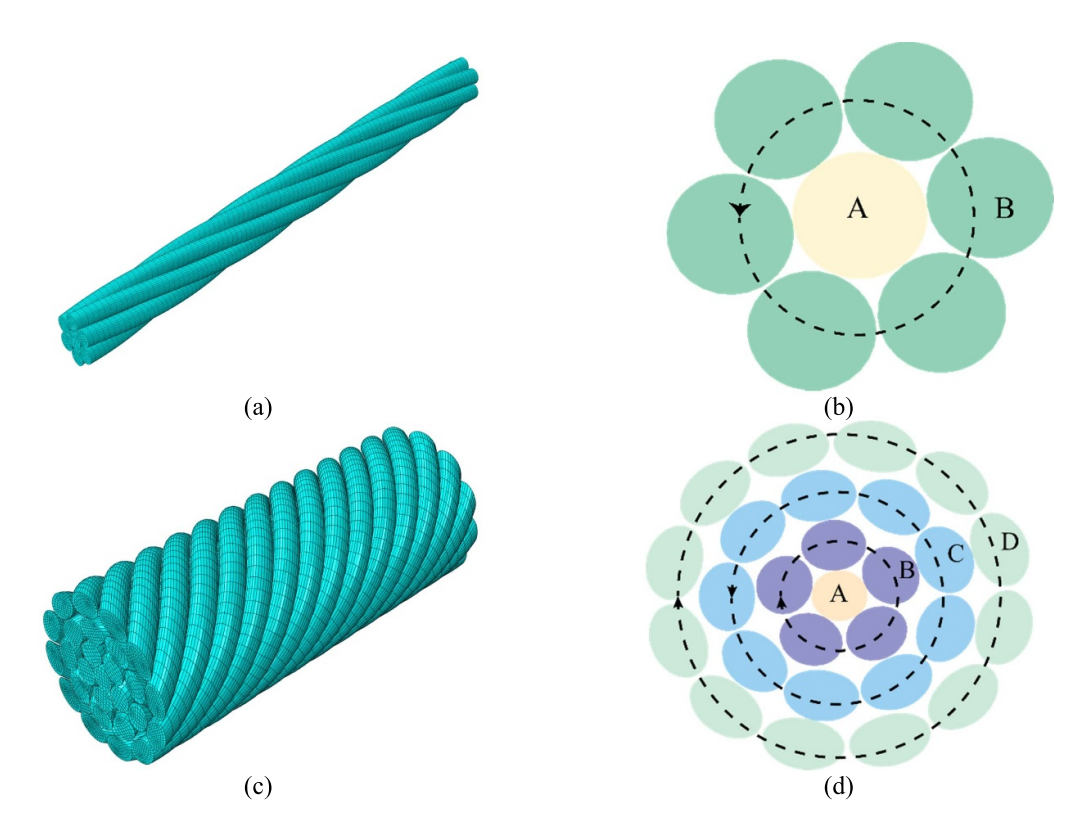


**Figure 8.** (a) Mesh representation of the  $1 \times 7$  and (b) the cross-sectional components of  $1 \times 7$ , (c) mesh representation of the  $1 \times 27$  and (d) cross-sectional components of the  $1 \times 27$ .

and unconstrained conditions are depicted in figures 9(a) and (b). It shows that both  $1 \times 7$  and  $1 \times 27$  SMP need significantly less force to achieve elongation when compared to solid bars considering the same volumes. At the same time, the cables show similar reduction in recovery force.

For the  $1 \times 7$  SMP cable, programming and cooling require an average force of approximately 90% compared to an equivalent volume of the solid SMP bar (figure 9(a)). While the average required force to elongate the  $1 \times 27$  SMP cable was 27% of the solid SMP bar.

The cables construction introduces inter-wire interactions that facilitate load sharing and stress distribution. These interwire interactions consequently bestow smoother and more efficient elongation capabilities mitigating stress concentration, which is more prevalent in solid bars upon thermomechanical loading. To acquire a deeper physical understanding of the performance of these SMP cables during recovery step, another investigation on analyzing the shape recovery process of both SMP cables and solid SMP bars may be carried out under 20% strain. The results reveal that there is no significant difference between these SMP configurations and their solid counterparts in the shape recovery path (figures 9(c) and (d)). This indicates that the shape memory properties or recovery ability of the SMP cables may not be affected even by complex configurations; thus, they still can preserve their functionalities.

It is noted that, as compared to SMAs, the recovery stress of SMPs is low, although the recovery strain of SMPs can be very high. Due to their higher recovery strain, some analyses show

that the recovery energy of SMPs can be comparable to or even higher than that of SMAs [59]. However, it is recognized that increasing the recovery stress of SMPs can further improve the performance of SMP cables. Several efforts have been made in the past years to enhance the recovery stress of SMPs. One approach is to use cold programming, i.e. programming in a glassy state. It is found that when the SMP is deformed to plastic deformation in a glassy state, it usually leads to higher recovery stress than programming in the rubbery state [60–63]. Another approach is to introduce higher steric hindrance to the SMP network, so that the programming energy can be stored by enthalpy increase through bond length change and bond angle change, in addition to the classical entropy reduction mechanism [64, 65]. It is found that this design strategy leads to much-improved recovery stress for both thermal curing and ultraviolet curing SMPs [66].

Following the above discussion and evaluating the shape recovery of SMP cable under finite deformation, figure 10 depicts the thermomechanical behavior of these cables under two strain levels of 20% and 40%. Both cable configurations exhibit a remarkable shape recovery in response to the applied strains. This behavior persists that even under a higher strain 40%, both configurations still demonstrate near complete shape recovery. To further characterize and quantify the shape memory properties of the SMP cables under 40% strain, the shape recovery ratio  $(R_r)$  and shape fixity ratio  $(R_f)$ —two important metrics for assessing shape memory performance—were calculated according to established formulas [28]:

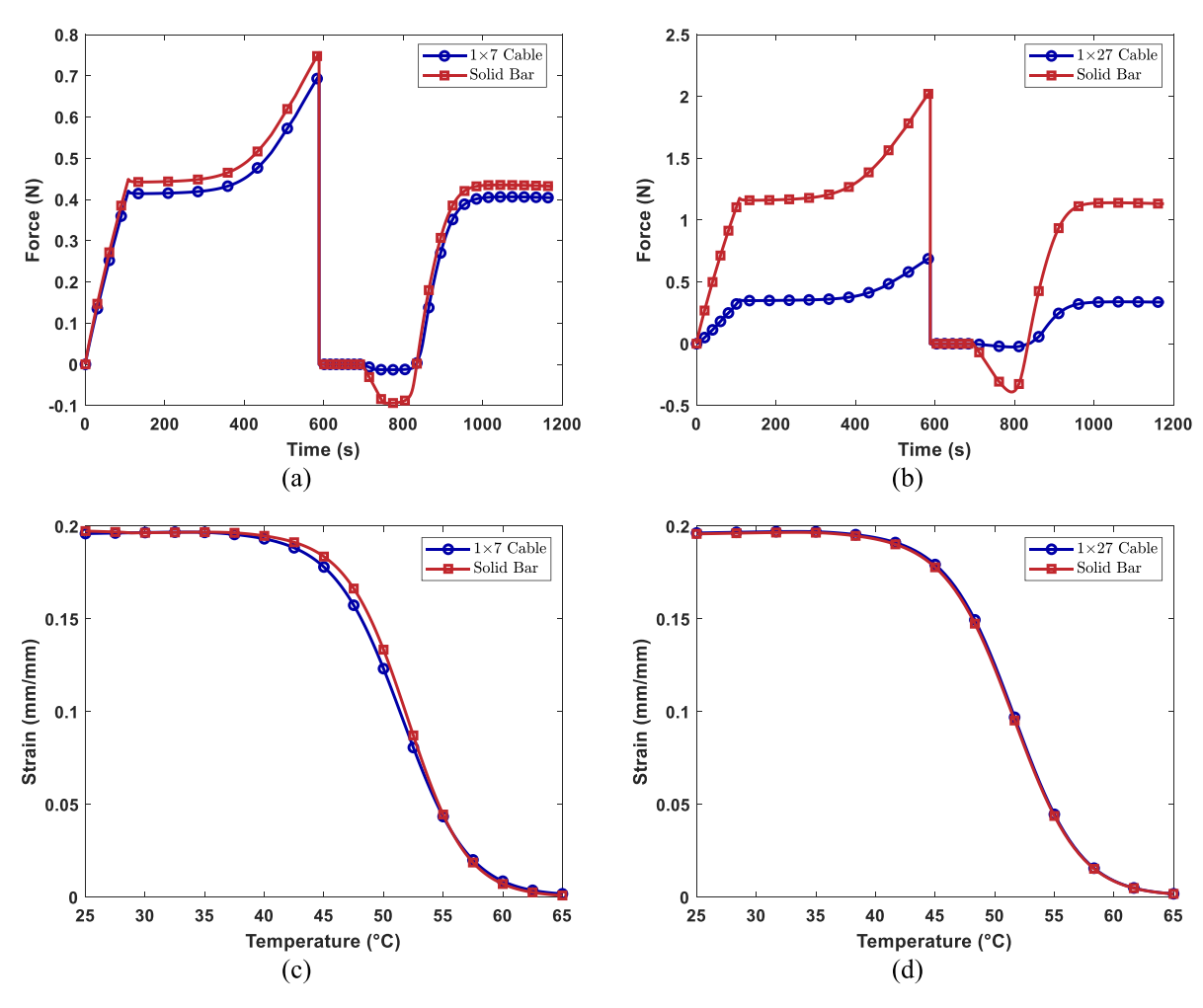


**Figure 9.** Force recovery profiles of SMP cable and solid SMP wire for (a)  $1 \times 7$ , (b)  $1 \times 27$ . Shape recovery trajectory of SMP cable and solid SMP wire for (c)  $1 \times 7$ , (d)  $1 \times 27$ .

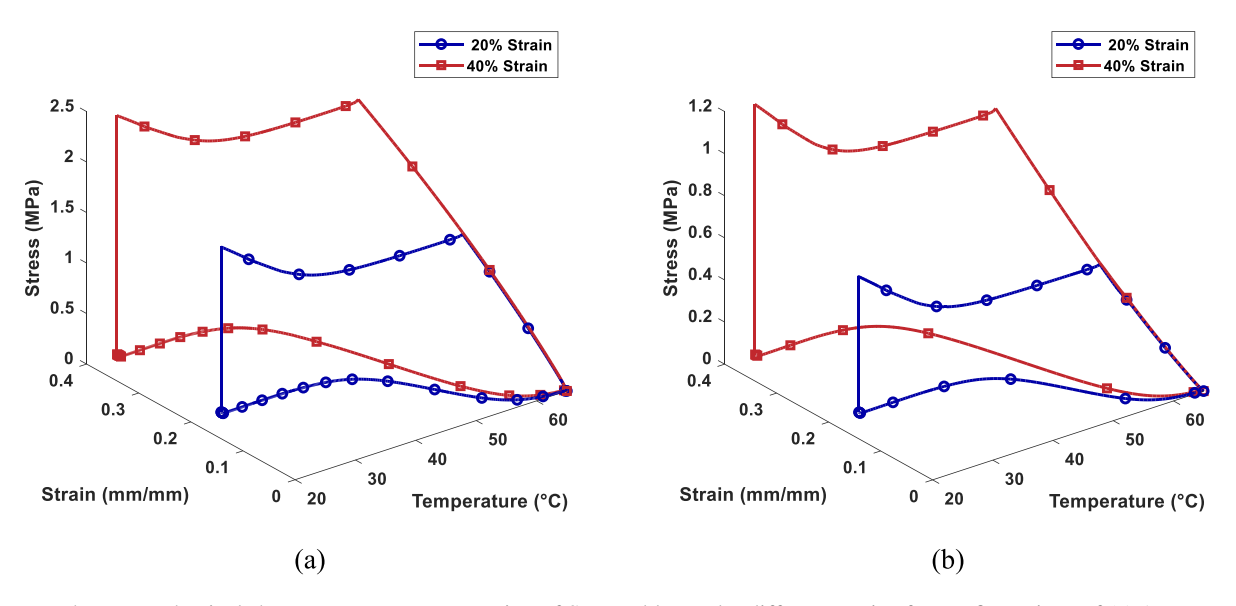


Figure 10. Thermomechanical shape recovery representation of SMP cables under different strains for configurations of (a)  $1 \times 7$ , and (b)  $1 \times 27$ .

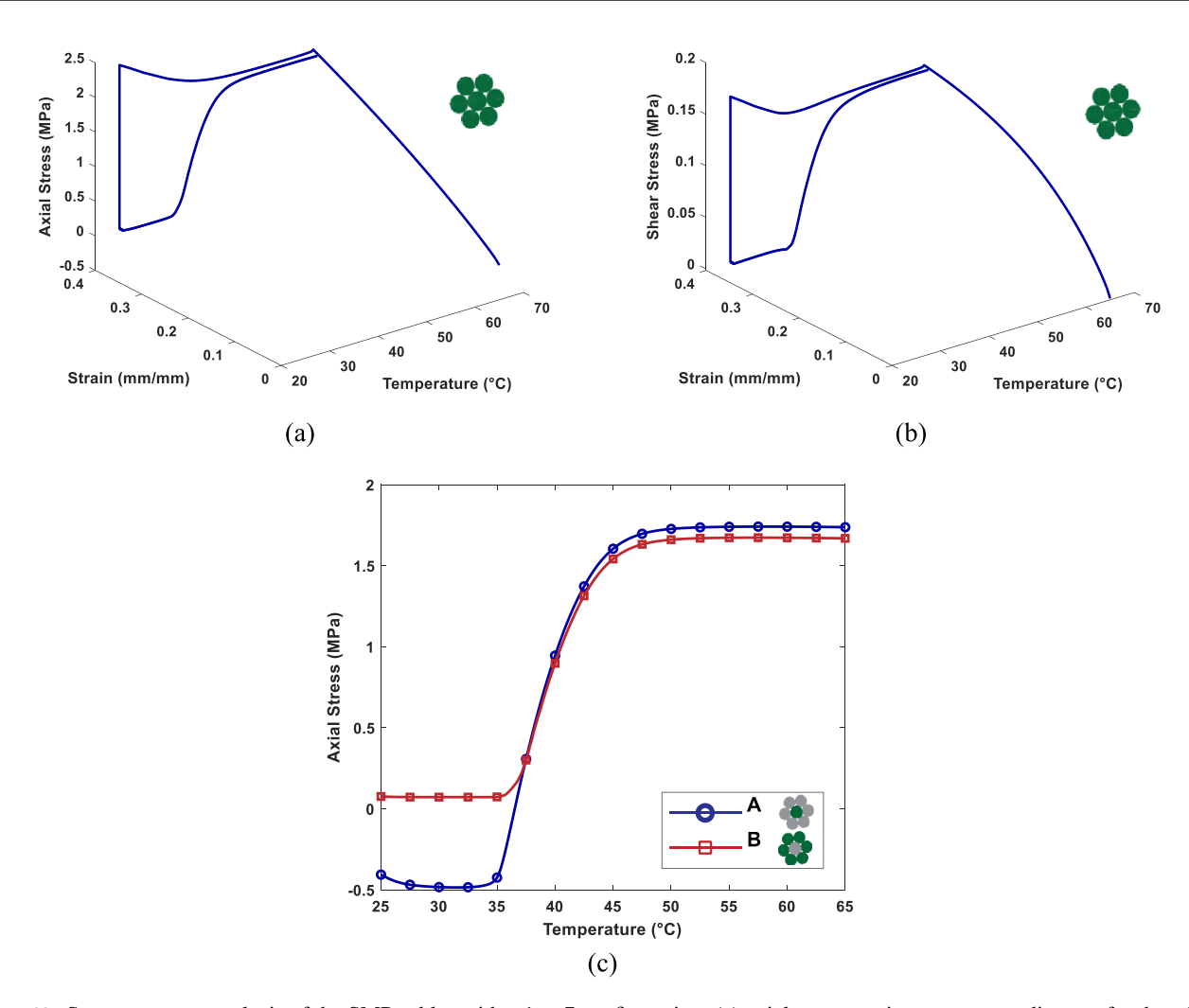


Figure 11. Stress recovery analysis of the SMP cables with a  $1 \times 7$  configuration: (a) axial stress-strain-temperature diagram for the whole cable, (b) of shear stress-strain-temperature diagram for whole cable, (c) Evaluation of the axial stress recovery of the  $1 \times 7$  SMP cable components.

$$R_r = \frac{\varepsilon_{\text{max}} - \varepsilon_p}{\varepsilon_{\text{max}}} \tag{19}$$

$$R_f = \frac{\varepsilon_u}{\varepsilon_{\text{max}}} \tag{20}$$

where  $\varepsilon_{\rm max}$  denotes the peak strain value reached at the end of the loading phase,  $\varepsilon_p$  represents the residual strain remaining after the thermomechanical cycle is complete, and  $\varepsilon_u$  quantifies the strain level upon unloading, when the applied load is removed.

The  $1 \times 7$  configuration and the  $1 \times 27$  SMP cable both achieve a shape recovery rate of 99.16%. However, their shape fixity values differ, with the  $1 \times 7$  configuration exhibiting a shape fixity of 97.9%, while the  $1 \times 27$  SMP cable demonstrates a higher shape fixity of 98.3%. Therefore, comparing the two cables' recovery behavior, it can be found that the number of layers and wires in the cables as well as the amount of applied deformation, may not significantly influence shape memory capabilities and have sufficient efficiency in returning to their original forms.

In the force recovery analysis of the SMP cables with a  $1 \times 7$  configuration, the stresses on the entire cable and each

of its parts are assessed in figures 11(a) and (b). It should be noted that the stresses are calculated using geometric attributes described in table 4. The results indicate that SMP cables possess outstanding capabilities in fully restoring both axial and shear loads. It is worth highlighting that for the  $1 \times 7$  configuration, the outer layer bears the main portion of the shear stress. Furthermore, figure 11(c) illustrates how the core wire initially exhibits a negative stress value during force recovery, owing to its inherent material properties and thermal characteristics. Gradually, upon heating, the stress in the core wire steadily rises, ultimately reaching the original 1.7 MPa stress level, providing clear evidence of a successful force recovery process. On the contrary, the outer layer, comprising six wires, highlights an initial positive stress response during force recovery. As the temperature rises, the stress within the outer layer approaches the baseline stress of 1.6 MPa, proving a successful force recovery as well. Nonetheless, the recovery force in the outer layer is slightly lower than that observed in the core wire. This can be attributed to the intricate interplay among the various wires of the outer layer, resulting in diverse mechanical responses compared to the behavior of the core wire. Furthermore, the evolution of von-Mises stress contours

**Table 4.** Geometric attributes of the  $1 \times 7$  and  $1 \times 27$  SMP cables and their components. Reprinted from [7], Copyright (2013), with permission from Elsevier.

	Type	N	r(mm)	d(mm)	$A_0 \left( \text{mm}^2 \right)$	$J_0\left(\mathrm{mm}^4 ight)$	D (mm)	$\varphi (\deg)$
1 × 7	A	1	_	0.295	0.068	$7.43 \times 10^{-04}$	0.1475	
	В	6	0.286	0.277	0.361	$3.30 \times 10^{-02}$	0.4245	+11.3
	Cable	7	_	_	0.429	$3.37 \times 10^{-02}$	0.4245	
	A	_	_	0.226	0.04	$2.56 \times 10^{-04}$	0.113	
	В	5	0.226	0.226	0.20	$1.15 \times 10^{-02}$	0.339	-30
$1 \times 27$	C	9	0.452	0.226	0.361	$7.60 \times 10^{-02}$	0.565	+42
	D	12	0.678	0.226	0.481	$2.24 \times 10^{-01}$	0.791	-47
	Cable	27	_	_	1.083	$3.12 \times 10^{-01}$	0.791	

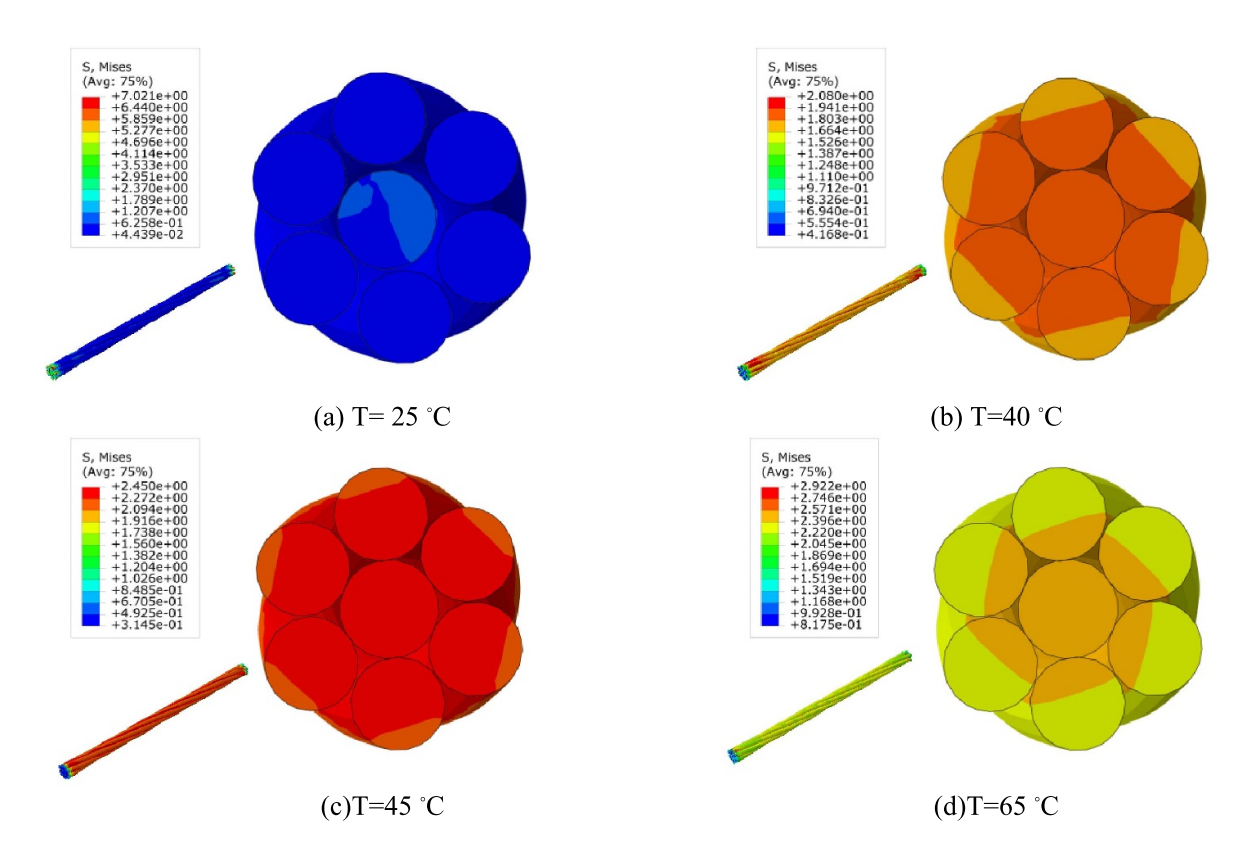
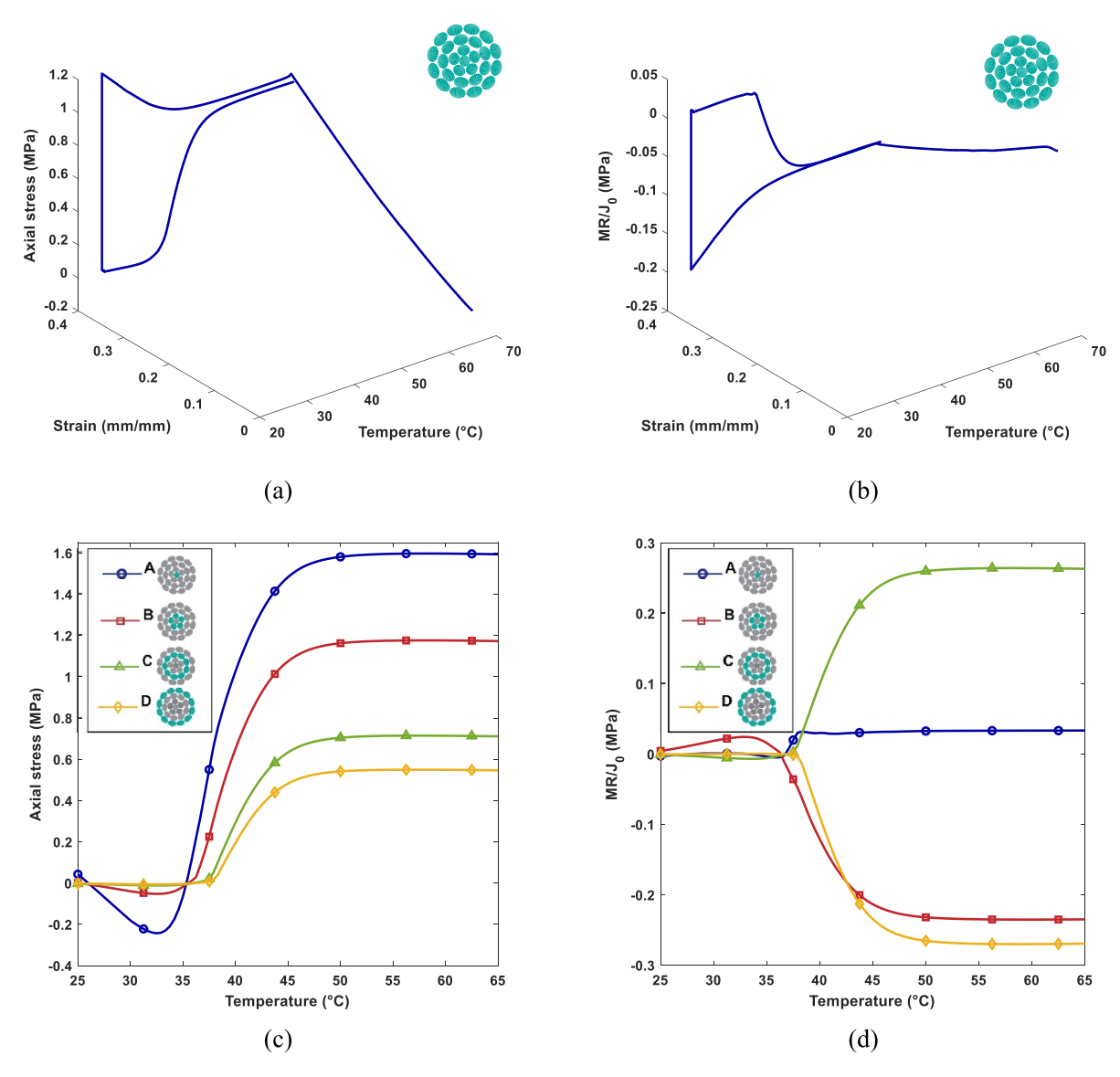


Figure 12. The evolution of von-Mises stress during recovery stages for the  $1 \times 7$  SMP cable under 40% applied strain and at the middle length.

at the middle of the wire rope under 40% axial strain for different temperatures of 25°C, 40°C, 45°C, 65°C are illustrated in figure 12. At room temperature, due to the temperature reduction as well as the effect of thermal contraction, the wires cannot fully be in the contact to their neighbors whereas at the higher temperatures they come into contact again and the induced stress recovery follows an increasing trend in this structure, in particular, around the cable core.

Figures 13 (a) and (b) present stress distribution for the  $1\times 27$  SMP cable specimen under 40% axial strain during force recovery. The  $1\times 27$  configuration restores both axial and shear loads similar to a  $1\times 7$  cable and exhibits negative shear stress as well. This phenomenon is a result of the prevalence of left-handed lay wires, which outnumber their right-handed lay counterparts. From figure 13(c), it becomes

evident that the core wire plays a vital role in the recovery process since it effectively endures significant normal stress. Consequently, the subsequent peak in the normal stress might be imparted to the B-type wire and the layers of C- and D-types. The distribution of shear stress in the inner layers is depicted in figure 13(d) as an outcome of the interplay between the wires in the outer layer. Examining the shear stress temperature diagram for individual components reveals that variations of lay direction profoundly affect the sign of shear stress. It implies that each layer in the shape memory cable contributes to the overall force recovery capability. This uniform behavior among the layers ensures that the cable maintains its structural integrity and functionality. Furthermore, in figures 14 and 15, respectively, the variation of longitudinal stress and displacement are depicted at different temperatures



**Figure 13.** Stress recovery analysis of the SMP cables with a  $1 \times 27$  configuration: (a) axial stress-strain-temperature diagram for whole cable, (b) shear stress-strain-temperature diagram for whole cable, (c) evaluation of the axial stress recovery of the  $1 \times 27$  SMP cable components, (d) evaluation of the shear stress recovery of the  $1 \times 27$  SMP cable components.

during recovery stages, indicating that the maximum stress recovery and axial deformation occur at the core and end of the cable, respectively.

The effects of temperature rate on the response of both configurations of SMP cables are depicted in figure 16. It describes the thermomechanical responses of SMP cables subjected to a pre-strain of 40%, under temperature rates of 5 and 1 °C min<sup>-1</sup>, respectively. The results showed diminished shape recovery at a higher rate, consistent with previous work showing that increased temperature rates typically reduce relaxation time for polymer chains during shape memory cycling [67]. This leads to additional residual stresses that hinder recovery.

To demonstrate the performance of SMP cables in terms of exhibiting a unique property known as multiple SME, a study is conducted under a specific loading scenario, which is investigated based on the conditions described in table 5 [50, 58, 68]. The strain-temperature-time diagram of the  $1\times27$  SMP cable under this investigation is illustrated in figure 17. To induce an initial temporary configuration (I), the cable at 55 °C is subjected to 1.1 mm deformation for about 40 s. With the strain sustained, the temperature is gradually lowered to 40 °C over 900s to set the temporary shape of the wire rope. Subsequently, an additional deformation is applied to the existing shape within 40 s, creating a second temporary shape labeled as (II). Maintaining the deformation

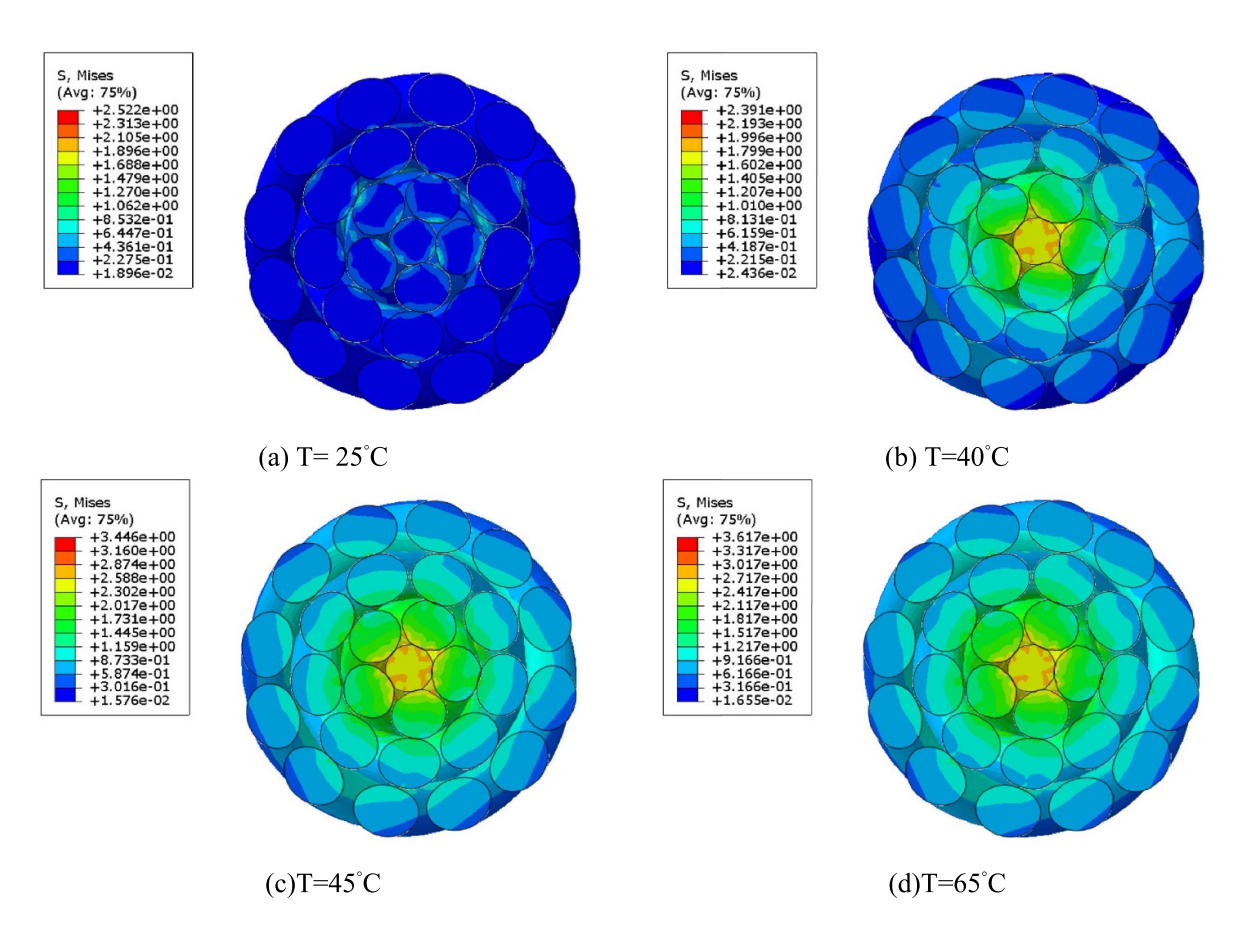


Figure 14. The evolution of von-Mises stress during recovery stages for  $1 \times 27$  SMP cable under 40% applied strain and at the middle length.

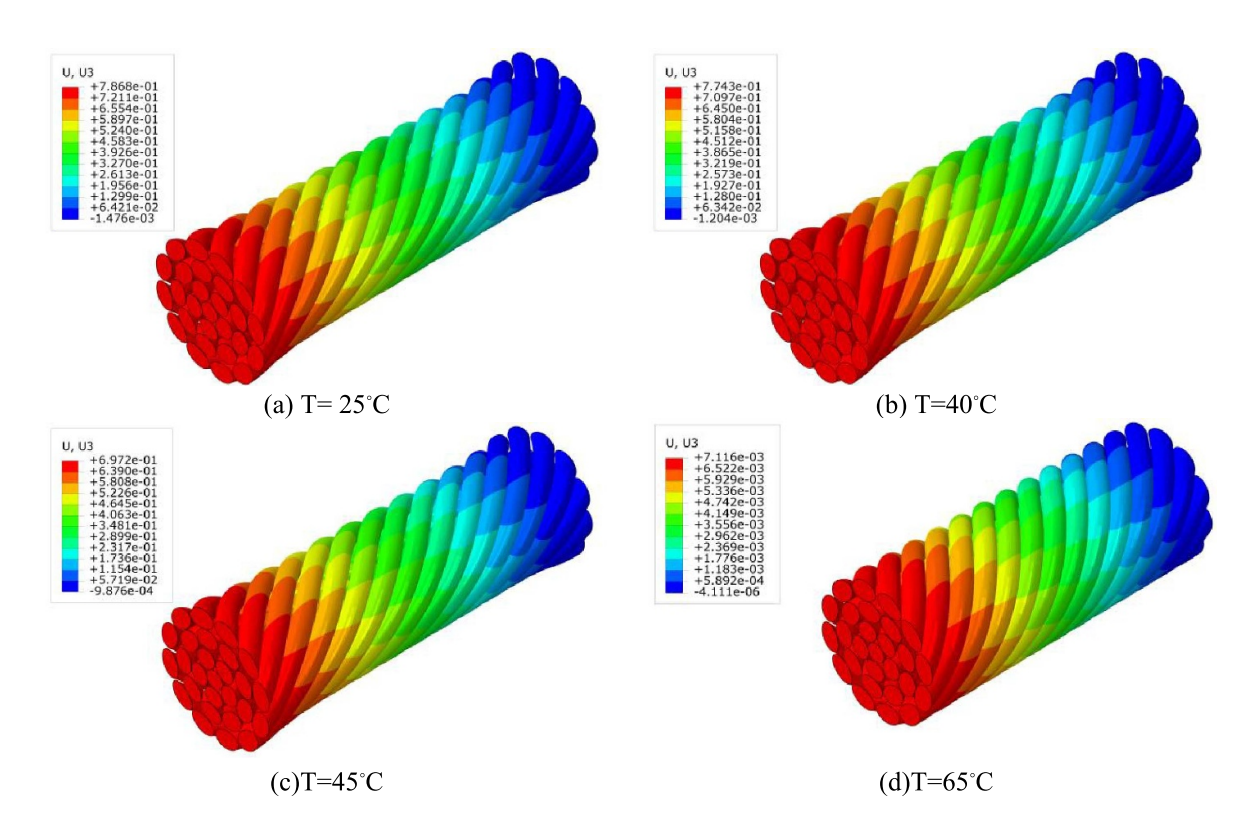
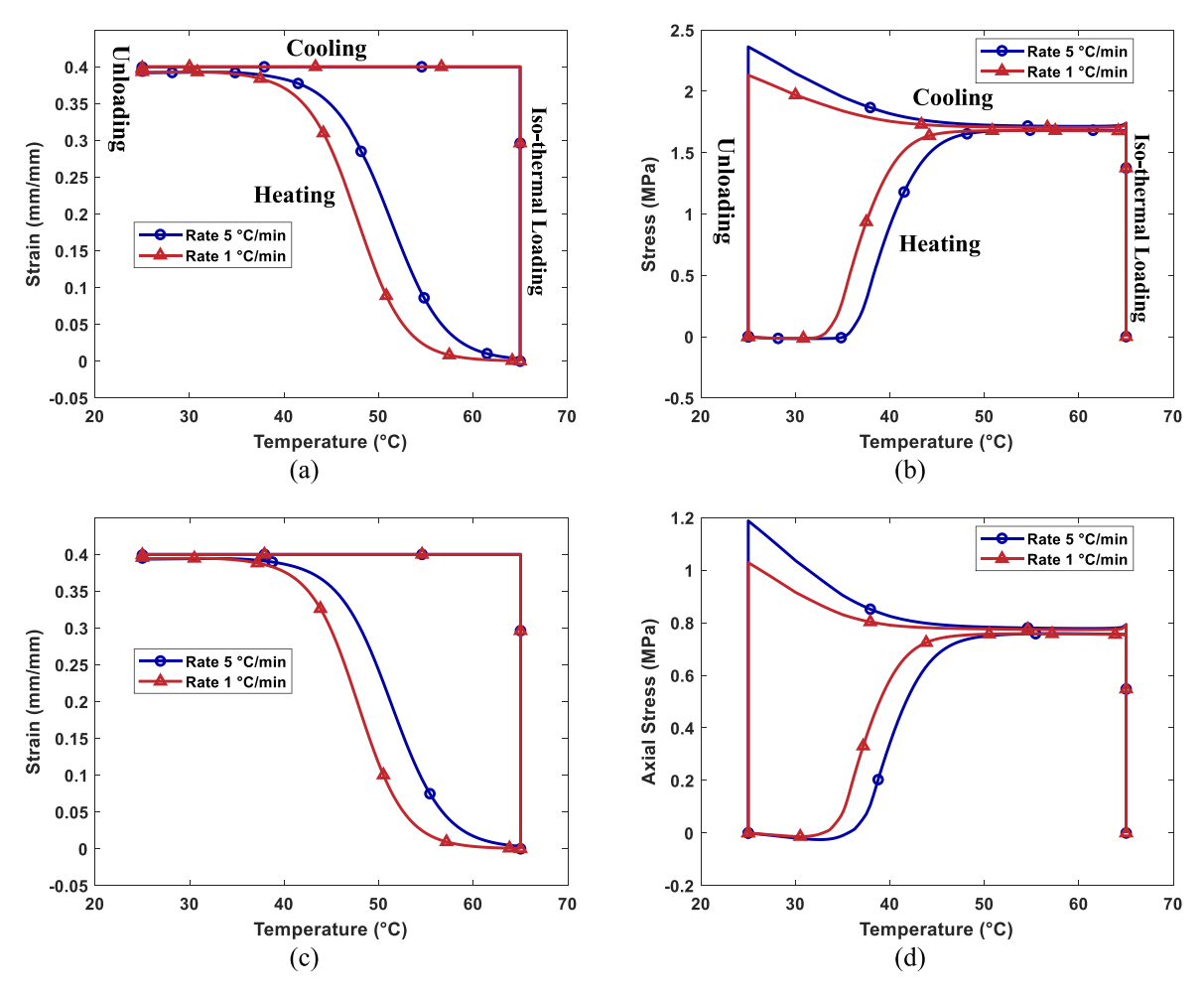


Figure 15. The variation of axial displacement during the shape recovery stage for the  $1 \times 27$  SMP cable under 20% applied strain.



**Figure 16.** Effect of temperate rate on the shape memory path for different SMP cables configurations: (a) shape recovery of the  $1 \times 7$  SMP cable, (b) force recovery of the  $1 \times 7$  SMP cable, (c) shape recovery of the  $1 \times 27$  SMP cable, (d) force recovery of the  $1 \times 27$  SMP cable.

Table 5. Loading scenario of triple-shape SME cycle. Reprinted from [59], Copyright (2021), with permission from Elsevier.

Step	First loading	First cooling	Second loading	Second cooling	Unloading	First shape recovery	Relaxation	Second shape recovery
Times (s)	40	900	40	1800	40	900	1800	1700
$T$ ( $^{\rm o}$ C)	55	$55 \rightarrow 40$	40	$40 \rightarrow 25$	25	$25 \rightarrow 40$	40	$40 \rightarrow 65$
$\delta  (\mathrm{mm})$	$0 \rightarrow 1.1$	1.1	$1.1 \rightarrow 2.3$	2.3	$\delta\left(t\right)$	$\delta\left(t\right)$	$\delta\left(t\right)$	$\delta\left(t\right)$

constant, the temperature may slowly decrease to 25 °C over 1800s. After this cooling period, the constraints are promptly removed within 40 s. These sequential steps constitute the shape programming process, facilitating the memorization of temporary shapes in the cables. Upon subjecting the SMP to a reheating process at a temperature of 40 °C, the initial temporary shape (III) is reinstated. Raising the temperature again to 55 °C allows the permanent shape to be regained (IV), effectively recalling the original structure. Moreover, a detailed representation of strain versus temperature over time can be found in figure 18. In two distinct steps, two different strain levels are applied to the SMP cable, allowing the successful retrieval of both temporary shapes. This

cyclic process not only facilitates the recovery of two temporary shapes but also holds promise for various other potential applications.

To complete the parametric study of the SMP cables, the influence of frictional coefficients variation on the required force to recover a  $1 \times 7$  SMP cable are analyzed when subjected to a 20% strain. The simulations encompass a wide range of polymer materials, with frictional coefficients ranging from 0.1 to 0.6 [69]. The result in figure 19 shows that the frictional coefficient has a negligible effect on the force recovery cycle. This result aligns with a previous study for SMA cables [1, 7] which also shows that no significant dependence on friction may be expected. The insensitivity to the frictional

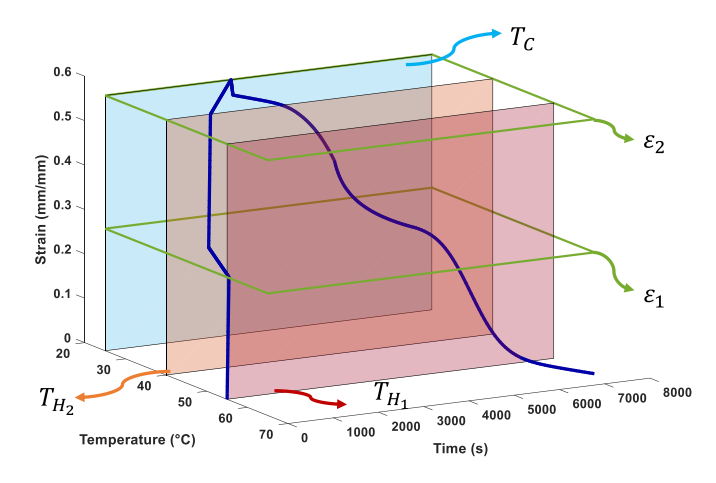


Figure 17. 3D strain-temperature-time diagram of thermo-mechanical shape recovery of the  $1 \times 27$  SMP cable for triple-shape SME.

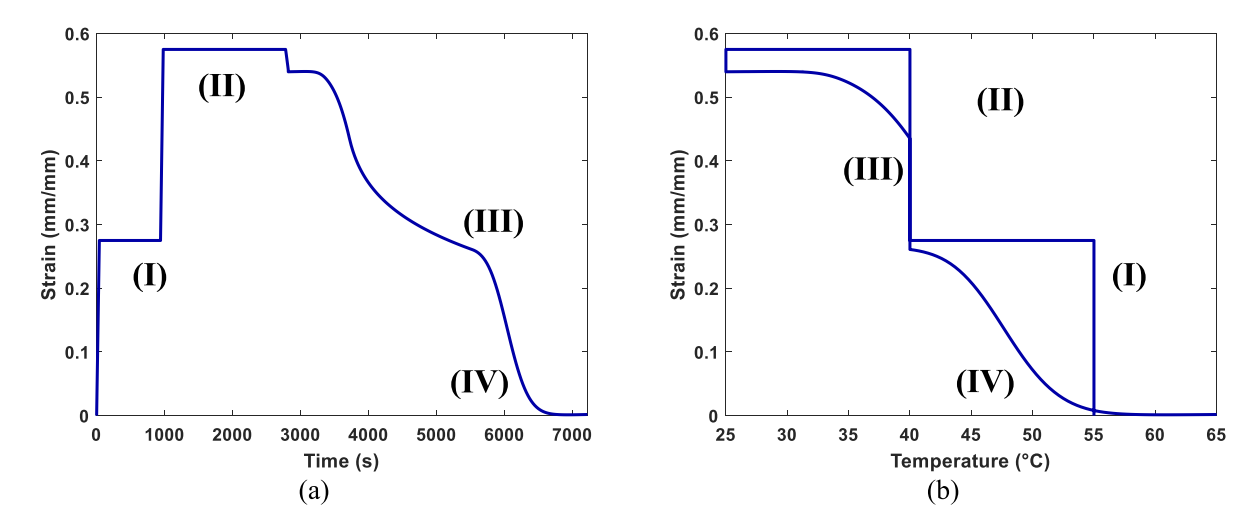


Figure 18. Thermomechanical characterization of shape memory behavior in a triple-SME for  $1 \times 27$  SMP cable: (a) strain-time response, and (b) strain-temperature.

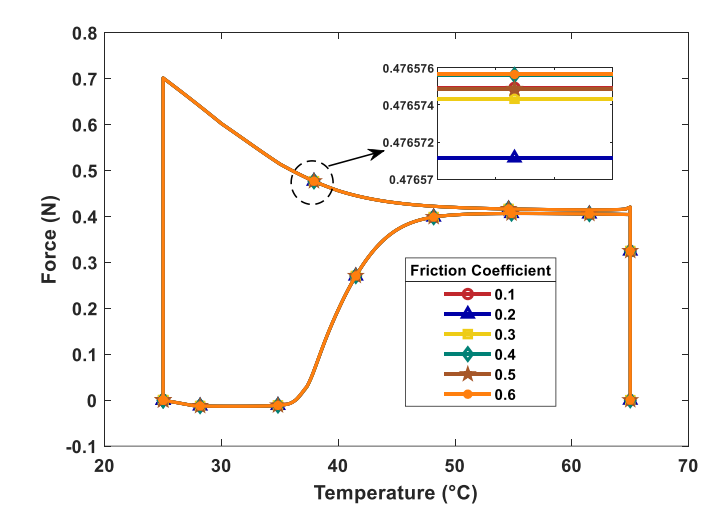


Figure 19. Effect of friction coefficient on the force recovery of  $1 \times 7$  SMP cable.

coefficient can be attributed to the fact that the majority of the applied strain is taken up in the axial elongation of the individual wires rather than inter-wire sliding [7]. At 20% over-

all cable strain, there is a minimal relative motion between the helically wound wires, thereby minimizing the frictional losses.

**Table 6.** Finite element models using factorial design with multiple control variable levels [1] [2002], reprinted by permission of the publisher (Taylor & Francis Ltd, www.tandfonline.com.).

Model	D(mm)	$\varphi (\deg)$
1	0.10	54.9
2	0.10	63.0
3	0.10	72.0
4	0.20	54.9
5	0.20	63.0
6	0.20	72.0
7	0.38	54.9
8	0.38	63.0
9	0.38	72.0

# 6. Optimization of a 1 $\times$ 6 SMP cable

In this section, the DOE methodology is employed for the  $1\times 6$  SMP cable to maximize the specific energy. The DOE approach involves a systematic variation of input parameters through a series of experiments or runs, enabling the identification of key factors influencing the response. Through purposeful adjustments of controllable variables, alterations in the output are determined, facilitating the attainment of the desirable optimization.

The output response in this FEA of SMP cables is the specific energy, denoted as  $\eta$ , and may be calculated by  $\eta = F$   $\Delta/M$ , in which F,  $\Delta$  and M denote, respectively, the recovered force, the cable displacement, and mass.

In the context of a single-layer configuration (refer to figure 2), the strand characteristics are influenced by three adjustable parameters: the wire diameter, helix angle, and core diameter. When considering an *n*-layer strand, the numbers of controllable factors expand to (2 n + 1). In a broader perspective, when dealing with this particular set of factors (2 n + 1) and each factor exhibiting k levels, the factorial design necessitates the execution of  $k^{2n+1}$  tests. In this investigation, FEA is undertaken considering three levels of factors. To expedite the computational efficiency of solutions, wire diameters for the two wire types are taken to be the same, in accordance with the standard industry guidelines outlined by Dynalloy trading company. The two primary adjustable variables are wire diameters of 0.10, 0.20, and 0.38 mm, and helix angles at settings of 54.9, 63.0, and 72.0 degrees. Consequently, based on factorial design, the present study considered 3<sup>2</sup> finite element analyses, as represented in table 6. It is worth noting that within the framework of the DOE approach, the dimensions of the element are deliberately selected to be sufficiently reduced to minimize errors associated with the meshed model, thereby ensuring the precision and reliability of the outcomes.

The cable-specific energy interpolation equation, which relies on controllable factors, is derived by acquiring output response data and subsequent computation using statistical design-expert software as:

$$\eta = 0.1999 + 0.0094D - 0.0395\varphi - 0.0174D\varphi + 0.0029D^{2} + 0.0195\varphi^{2} - 0.0029D^{2}\varphi + 0.0171D\varphi^{2}.$$
(21)

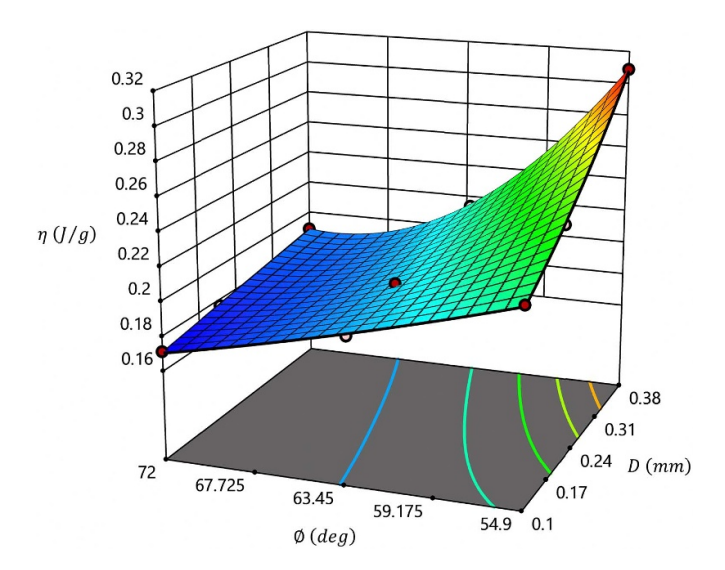


**Figure 20.** Variation of the specific energy for  $1 \times 6$  SMP cable plotted for different diameters and helix angles.

The 3D surface plot of the specific energy as a function of helix angle and diameter is illustrated in figure 20. It can be observed that increasing the helix angle leads to a reduction in specific energy while increasing the diameter results in higher specific energy values. At lower helix angles, the effect of diameter change on specific energy is more pronounced. The maximum specific energy from the response surface is attributed to model 7, which has a 0.38 mm diameter and a 54.9° helix angle. In contrast, model 3, with a 0.1 mm diameter and 72° helix angle, exhibits the lowest specific energy.

These findings demonstrate that helix angle and wire diameter significantly influence the specific energy performance of  $1 \times 6$  SMP cables. The insights gained can guide material selection and geometric design to achieve the desired balance of flexibility, deformability, and restoration force to maximize specific energy.

# 7. Summary and conclusions

This work introduces the concept of SMP cables for the first time and provides insights into the thermomechanical properties of SMP wire ropes and their components within the small and finite deformation regime. In order to validate modeling approaches, FEA is employed to simulate the intricate geometry and interwire contact interactions of a  $1 \times 37$  steel wire rope and compares against available results. Afterwards, a thermo-visco-hyperelastic constitutive model developed by Arrieta et al [50] is implemented due to its simplicity and agreement with experimental observations for simulating both the shape and stress recovery of SMPs under the uniaxial test. Subsequently, the thermo-mechanical properties and recovery characteristics of SMP cables with 1  $\times$  7 and 1  $\times$  27 configurations are analyzed. The cables have been subjected to an axial load, and their force recovery, shape recovery, and normal as well as shear stress distributions are evaluated under constrained and unconstrained conditions. Parametric analysis also investigates the effects of the frictional coefficient and pronounces the influence of temperature ramp rate on recovery performance. The dual and multiple shape memory phenomenon is also effectively characterized through sequential shape programming and recovery steps. Furthermore, DOE approach may be employed to optimize the geometry of a  $1\times 6$  SMP cable in order to maximize specific energy. The detailed analyses conducted on single helix SMP wire rope models with configurations of  $1\times 7$ ,  $1\times 27$ , and  $1\times 6$  in this study yield the following key findings:

- SMP cables require significantly less force for elongation compared to solid SMP bars with equivalent volume. For a 1 × 7 cable, the needed force is 90% of a solid bar, while for a 1 × 27 cable, it is only 27%.
- Both  $1 \times 7$  and  $1 \times 27$  SMP cable configurations exhibit remarkable shape recovery under different strain levels.
- The stress distribution varies between the core and outer wires during recovery due to the different geometric positions; however, full recovery is achieved in all components.
- The helix angle and wire diameter have a pronounced effect on the specific energy performance of SMP cables. Lower helix angles and larger diameters amplify the maximum specific energy. There might be about 80% difference between the minimum and maximum of induced specific energy of the 1 × 6 SMP cable.
- The study demonstrates the successful triple-SME in a 1 × 27 SMP cable, allowing for multiple temporary shapes and the recovery of the original structure.

While this study focuses on the thermomechanical properties of SMP cables using a specific acrylate polymer, the modeling approach can be applied to other SMP polymer systems. Different compositions may provide tailored properties and applications. Further experimental validation is needed to validate the findings and explore behavior using alternative polymers. Although we validated the SMP ropes by finite element modeling, future experimental testing is highly desired and should aim to expand understanding of thermomechanical behavior across polymer systems, which will be a topic of our next-step studies.

## Data availability statement

All data that support the findings of this study are included within the article (and any supplementary files).

## **Funding**

A O and G L acknowledge the support by the US National Science Foundation under Grant Number OIA-1946231 and the Louisiana Board of Regents for the Louisiana Materials Design Alliance (LAMDA).

#### **Author contributions**

Alireza Enferadi: Conceptualization, Methodology, Writing-Original draft preparation, Software, Visualization, Alireza Ostadrahimi: Methodology, Visualization, Reviewing and editing, Guoqiang Li: Supervision, Reviewing and editing, Majid Baniasadi: Visualization, Reviewing and editing, Mostafa Baghani: Supervision, Reviewing and editing.

#### Conflict of interest

The authors declare that they have no known competing financial interests or personal relationships that could have appeared to influence the work reported in this paper.

#### **ORCID iDs**

Alireza Enferadi https://orcid.org/0000-0002-1962-5436 Alireza Ostadrahimi https://orcid.org/0000-0002-1179-4833

Guoqiang Li https://orcid.org/0000-0002-7004-6659 Majid Baniassadi https://orcid.org/0000-0002-4434-082X Mostafa Baghani https://orcid.org/0000-0001-6695-3128

#### References

- [1] Vahidi S, Arghavani J, Choi E and Ostadrahimi A 2022 Mechanical response of single and double-helix SMA wire ropes Mech. Adv. Mater. Struct. 29 5393–406
- [2] Costello G A 1997 Theory of Wire Rope (Mechanical Engineering Series) (Springer Science & Business Media)
- [3] Utting W S and Jones N 1987 The response of wire rope strands to axial tensile loads—Part I. Experimental results and theoretical predictions *Int. J. Mech. Sci.* 29 605–19
- [4] Stanova E, Fedorko G, Fabian M and Kmet S 2011 Computer modelling of wire strands and ropes Part I: theory and computer implementation Adv. Eng. Softw. 42 305–15
- [5] Stanova E, Fedorko G, Fabian M and Kmet S 2011 Computer modelling of wire strands and ropes part II: finite element-based applications Adv. Eng. Softw. 42 322–31
- [6] Wang D, Zhang D, Wang S and Ge S 2013 Finite element analysis of hoisting rope and fretting wear evolution and fatigue life estimation of steel wires *Eng. Fail. Anal.* 27 173–93
- [7] Reedlunn B, Daly S and Shaw J 2013 Superelastic shape memory alloy cables: part II—Subcomponent isothermal responses *Int. J. Solids Struct.* 50 3027–44
- [8] Reedlunn B, Daly S and Shaw J 2013 Superelastic shape memory alloy cables: part I–Isothermal tension experiments *Int. J. Solids Struct.* 50 3009–26
- [9] Biggs D and Shaw J 2016 Experimental characterization of shape memory alloy actuator cables *Proc. SPIE* 9800 79–90
- [10] Ozbulut O E, Daghash S and Sherif M M 2016 Shape memory alloy cables for structural applications *J. Mater. Civ. Eng.* 28 04015176
- [11] Sherif M M and Ozbulut O E 2018 Tensile and superelastic fatigue characterization of NiTi shape memory cables Smart Mater. Struct. 27 015007
- [12] Carboni B, Lacarbonara W and Auricchio F 2015 Hysteresis of multiconfiguration assemblies of nitinol and steel strands: experiments and phenomenological identification *J. Eng. Mech.* 141 04014135

- [13] Fang C, Zheng Y, Chen J, Yam M C H and Wang W 2019 Superelastic NiTi SMA cables: thermal-mechanical behavior, hysteretic modelling and seismic application *Eng.* Struct. 183 533–49
- [14] Shi F, Ozbulut O E, Li Z, Wu Z, Ren F and Zhou Y 2022 Effects of ambient temperature on cyclic response and functional fatigue of shape memory alloy cables *J. Build. Eng.* 52 104340
- [15] Yang X, Zhou H, Yang X, Zhou X, Zhang S Y and Du Y 2021 Shape memory alloy strands as cross-ties: fatigue behavior and model-cable net tests Eng. Struct. 245 112828
- [16] Dong H, Du X and Han Q 2019 Seismic responses of steel frame structures with self-centering energy dissipation braced on shape memory alloy cables Adv. Struct. Eng. 22 2136–48
- [17] Shi F, Ozbulut O E and Zhou Y 2020 Influence of shape memory alloy brace design parameters on seismic performance of self-centering steel frame buildings *Struct*. *Control Health Monit.* 27 e2462
- [18] Shi F, Saygili G, Ozbulut O E and Zhou Y 2020 Risk-based mainshock-aftershock performance assessment of SMA braced steel frames *Eng. Struct.* 212 110506
- [19] Liang D, Zheng Y, Fang C, Yam M C H and Zhang C 2020 Shape memory alloy (SMA)-cable-controlled sliding bearings: development, testing, and system behavior *Smart Mater. Struct.* 29 085006
- [20] Cao S, Ozbulut O E, Shi F and Deng J 2022 Experimental and numerical investigations on hysteretic response of a multi-level SMA/lead rubber bearing seismic isolation system *Smart Mater. Struct.* 31 035024
- [21] Teimouri A, Barbaz Isfahani R, Saber-Samandari S and Salehi M 2022 Experimental and numerical investigation on the effect of core-shell microcapsule sizes on mechanical properties of microcapsule-based polymers *J. Compos. Mater.* 56 2879–94
- [22] Deng J, Hu F, Ozbulut O E and Cao S 2022 Verification of multi-level SMA/lead rubber bearing isolation system for seismic protection of bridges *Soil Dyn. Earthq. Eng.* 161 107380
- [23] Fang C, Liang D, Zheng Y and Lu S 2022 Seismic performance of bridges with novel SMA cable-restrained high damping rubber bearings against near-fault ground motions *Earthq. Eng. Struct. Dyn.* 51 44–65
- [24] Shi F, Zhou Y, Ozbulut O E and Cao S 2021 Development and experimental validation of anchorage systems for shape memory alloy cables *Eng. Struct.* 228 111611
- [25] Silva P C S, Grassi E N D, Araújo C J, Delgado J M P Q and Lima A G B 2022 NiTi SMA superelastic micro cables: thermomechanical behavior and fatigue life under dynamic loadings Sensors 22 8045
- [26] Hisaaki T, Hisashi H, Etsuko Y and Shunichi H 1996 Thermomechanical properties in a thin film of shape memory polymer of polyurethane series *Smart Mater. Struct.* 5 483
- [27] Lendlein A and Kelch S 2002 Shape-memory polymers Angew. Chem., Int. Ed. 41 2034–57
- [28] Staszczak M, Nabavian Kalat M, Golasiński K M, Urbański L, Takeda K, Matsui R and Pieczyska E A 2022 Characterization of polyurethane shape memory polymer and determination of shape fixity and shape recovery in subsequent thermomechanical cycles *Polymers* 14 4775
- [29] Wang Y, Zhang J, Li M, Lei M, Wang Y and Wei Q 2022 3D printing thermo-responsive shape memory polymer composite based on PCL/TPU blends J. Polym. Res. 29 243
- [30] Testa P, Style R W, Cui J, Donnelly C, Borisova E, Derlet P M, Dufresne E R and Heyderman L J 2019 Magnetically addressable shape-memory and stiffening in a composite elastomer Adv. Mater. 31 1900561

- [31] Paudel A, Kuchena S F and Wang Y 2023 A full metal-free battery operating under cold condition enabled by an antisolvent *Electrochim. Acta* 469 143227
- [32] Wan X, Zhang F, Liu Y and Leng J 2019 CNT-based electro-responsive shape memory functionalized 3D printed nanocomposites for liquid sensors *Carbon* 155 77–87
- [33] Sodhi J S, Cruz P R and Rao I J 2015 Inhomogeneous deformations of light activated shape memory polymers *Int.* J. Eng. Sci. 89 1–17
- [34] Cehula J and Průša V 2020 Computer modelling of origami-like structures made of light activated shape memory polymers *Int. J. Eng. Sci.* 150 103235
- [35] Lu H, Lu C, Huang W M and Leng J 2016 Quantitative separation of the influence of copper (II) chloride mass migration on the chemo-responsive shape memory effect in polyurethane shape memory polymer *Smart Mater. Struct.* 25 105003
- [36] Yang J, Zheng Y, Sheng L, Chen H, Zhao L, Yu W, Zhao K-Q and Hu P 2018 Water induced shape memory and healing effects by introducing carboxymethyl cellulose sodium into Poly(vinyl alcohol) *Ind. Eng. Chem. Res.* **57** 15046–53
- [37] Jang J H, Hong S B, Kim J-G, Goo N S, Lee H and Yu W-R 2019 Long-term properties of carbon fiber-reinforced shape memory epoxy/polymer composites exposed to vacuum and ultraviolet radiation *Smart Mater. Struct.* 28 115013
- [38] Melly S K, Liu L, Liu Y and Leng J 2020 Active composites based on shape memory polymers: overview, fabrication methods, applications, and future prospects J. Mater. Sci. 55 10975–1051
- [39] Baghani M, Baniassadi M and Rémond Y 2023

  Computational Modeling of Intelligent Soft Matter: Shape
  Memory Polymers and Hydrogels (Elsevier)
- [40] Gong X, Xie F, Liu L, Liu Y and Leng J 2020 Electro-active variable-stiffness corrugated structure based on shape-memory polymer composite *Polymers* 12 387
- [41] Sun J, Peng B, Lu Y, Zhang X, Wei J, Zhu C and Yu Y 2022 A photoorganizable triple shape memory polymer for deployable devices *Small* 18 2106443
- [42] Ansari M, Golzar M, Baghani M, Abbasishirsavar M and Taghavimehr M 2019 Force recovery evaluation of thermo-induced shape-memory polymer stent: material, process and thermo-viscoelastic characterization *Smart Mater. Struct.* 28 095022
- [43] Biswas M C, Chakraborty S, Bhattacharjee A and Mohammed Z 2021 4D printing of shape memory materials for textiles: mechanism, mathematical modeling, and challenges Adv. Funct. Mater. 31 2100257
- [44] Enferadi A, Baniassadi M and Baghani M 2023 Innovative multiphysics approach for designing high-performance thermo-responsive shape memory polymer microvalve Eur. J. Mech. A 103 105174
- [45] Li G, Meng H and Hu J 2012 Healable thermoset polymer composite embedded with stimuli-responsive fibres *J. R. Soc. Interface* **9** 3279–87
- [46] Yang Q and Li G 2014 Spider-silk-like shape memory polymer fiber for vibration damping Smart Mater. Struct. 23 105032
- [47] Sharafi S and Li G 2016 Multiscale modeling of vibration damping response of shape memory polymer fibers *Composites* B **91** 306–14
- [48] Fan J and Li G 2017 High performance and tunable artificial muscle based on two-way shape memory polymer RSC Adv. 7 1127–36
- [49] Yang Q, Fan J and Li G 2016 Artificial muscles made of chiral two-way shape memory polymer fibers Appl. Phys. Lett. 109 183701
- [50] Arrieta S, Diani J and Gilormini P 2014 Experimental characterization and thermoviscoelastic modeling of strain and stress recoveries of an amorphous polymer network *Mech. Mater.* 68 95–103

- [51] Yarali E, Taheri A and Baghani M 2020 A comprehensive review on thermomechanical constitutive models for shape memory polymers J. Intell. Mater. Syst. Struct. 31 1243–83
- [52] Baniasadi M, Foyouzat A and Baghani M 2020 Multiple shape memory effect for smart helical springs with variable stiffness over time and temperature *Int. J. Mech. Sci.* 182 105742
- [53] Westbrook K K, Kao P H, Castro F, Ding Y and Jerry Qi H 2011 A 3D finite deformation constitutive model for amorphous shape memory polymers: a multi-branch modeling approach for nonequilibrium relaxation processes *Mech. Mater.* 43 853–69
- [54] Diani J, Gilormini P, Frédy C and Rousseau I 2012 Predicting thermal shape memory of crosslinked polymer networks from linear viscoelasticity *Int. J. Solids Struct.* 49 793–9
- [55] Williams M L, Landel R F and Ferry J D 1955 The temperature dependence of relaxation mechanisms in amorphous polymers and other glass-forming liquids J. Am. Chem. Soc. 77 3701–7
- [56] Xie T 2010 Tunable polymer multi-shape memory effect Nature 464 267–70
- [57] Yu K, Xie T, Leng J, Ding Y and Qi H J 2012 Mechanisms of multi-shape memory effects and associated energy release in shape memory polymers Soft Matter 8 5687–95
- [58] Bakhtiyari A, Baniasadi M and Baghani M 2021 Development of a large strain formulation for multiple shape-memory-effect of polymers under bending *Int. J. Mech. Sci.* 204 106560
- [59] Li G 2014 Self-Healing Composites: Shape Memory Polymer Based Structures (Wiley)
- [60] Mao Y, Robertson J M, Mu X, Mather P T and Jerry Qi H 2015 Thermoviscoplastic behaviors of anisotropic shape

- memory elastomeric composites for cold programmed non-affine shape change *J. Mech. Phys. Solids* **85** 219–44
- [61] Li G and Xu W 2011 Thermomechanical behavior of thermoset shape memory polymer programmed by cold-compression: testing and constitutive modeling *J. Mech. Phys. Solids* 59 1231–50
- [62] Li G and Wang A 2016 Cold, warm, and hot programming of shape memory polymers J. Polym. Sci. B 54 1319–39
- [63] Dai L, Tian C and Xiao R 2020 Modeling the thermo-mechanical behavior and constrained recovery performance of cold-programmed amorphous shape-memory polymers Int. J. Plast. 127 102654
- [64] Wick C D, Peters A J and Li G 2021 Quantifying the contributions of energy storage in a thermoset shape memory polymer with high stress recovery: a molecular dynamics study *Polymer* 213 123319
- [65] Fan J and Li G 2018 High enthalpy storage thermoset network with giant stress and energy output in rubbery state *Nat. Commun.* 9 642
- [66] Feng X and Li G 2021 High-temperature shape memory photopolymer with intrinsic flame retardancy and record-high recovery stress Appl. Mater. Today 23 101056
- [67] Nguyen T D, Jerry Qi H, Castro F and Long K N 2008 A thermoviscoelastic model for amorphous shape memory polymers: incorporating structural and stress relaxation J. Mech. Phys. Solids 56 2792–814
- [68] Baniasadi M, Maleki-Bigdeli M-A and Baghani M 2020 Force and multiple-shape-recovery in shape-memory-polymers under finite deformation torsion-extension *Smart Mater*. Struct. 29 055011
- [69] Brydson J A 1999 Plastics Materials (Elsevier)